

Floquet simulators for topological surface states in isolation

Kun Woo Kim^{1,2}, Dmitry Bagrets¹, Tobias Micklitz³, Alexander Altland¹

¹*Institut für Theoretische Physik, Universität zu Köln, Zùlpicher Straße 77, 50937 Köln, Germany*

²*Department of Physics, Chung-Ang University, 06974 Seoul, Republic of Korea*

³*Centro Brasileiro de Pesquisas Físicas, Rua Xavier Sigaud 150, 22290-180, Rio de Janeiro, Brazil*

(Dated: January 12, 2023)

We propose dynamical protocols allowing for the engineered realization of topological surface states in isolation. Our approach builds on the concept of synthetic dimensions generated by driving systems with incommensurate frequencies. As a concrete example, we consider 3d topological surface states of a 4d quantum Hall insulator via a $(1 + 2_{\text{syn}})$ -dimensional protocol. We present first principle analytical calculations demonstrating that no supporting 4d bulk phase is required for a 3d topological surface phase. We back the analytical approach by numerical simulations and present a detailed blueprint for the realization of the synthetic surface phase with existing quantum linear optical network device technology. We then discuss generalizations, including a proposal for a quantum simulator of the $(1 + 1_{\text{syn}})$ -dimensional surface of the common 3d topological insulator.

I. INTRODUCTION

Surface states of topological insulators (TI) define one of the most fascinating forms of quantum matter. Depending on their symmetries and dimensionality, they conduct charge, spin, or heat with topological protection against the detrimental effects of impurity scattering or interactions. These features make the TI surface distinct from any other form of quantum matter, and are believed to harbor far-reaching potential future device applications. At the same time, our understanding of the TI surface physics remains incomplete, both experimentally and theoretically. For example, even in the absence of interactions their conduction properties are not known quantitatively, and according to recent numerical work [1] even enigmatic. The experimental analysis of surface transport is hindered by the inevitable presence of an “insulating” bulk, with quotation marks because heat or electric currents easily leak away from the surface hindering a clear separation of surface and bulk currents.

According to the bulk–boundary principle, no *lattice* quantum system in isolation can be in the universality class of the TI surface. The necessity of a supporting bulk follows from topological band theory or, more fundamentally, as a consequence of anomaly inflow. The main message of this paper is that this no-go theorem can be sidestepped within the wider framework of Floquet quantum matter. Specifically, we will propose realizations of (dynamical) synthetic matter in universality classes indistinguishable from those of *isolated* (static) TI surfaces in the presence of effective disorder. Our work includes three novel conceptual elements: (i) the encoding of two and three dimensional surface state topologies in multi-frequency dynamical protocols, (ii) the first principle demonstration of the equivalence between the quantum states engineered in this way and insulator surface states, and (iii) the formulation of a detailed experimental blueprint suggesting that this program can be implemented in realistic devices within the framework of current date technology.

Previous work [2, 3] indeed pointed out the realizability

of topological metallic phases in dynamically driven lattice systems. However, the presence of a lattice structure made these systems subject to the notorious fermion doubling principle, which requires an even number of Dirac cones in the Floquet Brillouin zone. In the presence of impurities these mutually gap out, spoiling the surface state analogy. In order to realize a genuine surface state in isolation, a more radical departure from the solid state crystal paradigm is required. In this paper, we demonstrate that the toolbox of quantum optics contains platforms that are up to this task, optical lattices [4, 5], or linear optical networks [6–8] driven by multiple incommensurate frequencies. The driving of d -dimensional realizations of such systems by d_{syn} incommensurate frequencies is microscopically identical to a time periodic (Floquet) dynamics acting in an effective system of dimensionality $d + d_{\text{syn}}$ [9], where the structure of the Floquet operator in the d physical and d_{syn} synthetic dimensions depends on the driving protocol. Importantly, the correlations in the synthetic directions are not confined by the fermion doubling theorem, and this will be key to the engineering of topological surface states in isolation. We will label the $d + d_{\text{syn}}$ -dimensional Floquet metallic (FM) systems realized in this way as $\text{FM}_{d+d_{\text{syn}}}$ throughout.

The simulation of higher dimensional systems via driven low dimensional physical platforms is experimental reality. In breakthrough experiments it was applied to extend one-dimensional Anderson localization in the quantum kicked rotor [10–13] to higher dimensions. This defined an effectively disordered FM_{1+2} and led to the first high precision observation of a three-dimensional Anderson transition under parametrically controlled conditions [4, 14].

However, the realization of the TI surface states addressed in this paper requires the additional structure of an internal bi-valued degree of freedom or ‘spin’. (For earlier proposals to realize topological quantum matter with synthetic dimensions via the driving of systems with internal degrees of freedom, see Refs. [15] and [16]. Specifically, we need full control over the lattice nearest neighbor hopping for a system with two internal degrees

of freedom (“spin”). The required technology is not yet realized for the optical lattice [17] but is available in the alternative platform of linear optical networks [18]. We will therefore focus on this hardware and discuss the implementation of a $\text{FM}_{1+1_{\text{syn}}}$ and a $\text{FM}_{1+2_{\text{syn}}}$ TI surface state. We will demonstrate by numerical control simulations that unique signatures of surface state delocalization in the synthetic disordered system are observable for experimentally accessible time and length scales.

A further hallmark of our approach is that it realizes surfaces in effectively “disordered” phases lacking translational invariance. The reason is that the generation of synthetic dimension requires non-commuting operators both in synthetic and physical space. The simultaneous presence of these operators in the dynamics leads to non-integrability and chaotic fluctuations, physically equivalent to tunable disorder at mesoscopic length scales. Our approach, thus, simulates the surfaces of disordered topological quantum matter, which one may take as an added element of realism.

The plan of the paper is as follows. In Section II, we present dynamical protocols of $1d$ quantum walks that utilize synthetic dimensions to simulate higher dimensional systems. In Section III we introduce a quantum simulator of topological insulator surface states in isolation at the example of the $4d$ quantum Hall insulator. We introduce a $1d$ quantum walk protocol, discuss its topological property, and report on numerical simulations of the protocol, all supporting the idea that the surface states of the $4d$ quantum Hall insulator can be simulated by the $1d$ quantum walk. We then discuss a concrete blueprint, realizing the quantum walk within existing optical linear network set-up. Section IV provides further details and discusses generalizations. Specifically, we introduce a simulator of surface states of a $3d$ quantum spin Hall insulator. We conclude in Section VI. Aiming to keep the presentation as non-technical as possible, the details of various derivations are relegated to the Appendices.

II. DYNAMICAL PROTOCOLS

Consider the quantum walk of a spin-1/2 particle on a $1d$ lattice, generated by successive applications of translations and spin rotations. The single time-step evolution operator is of the general form

$$\hat{U}_t = \sum_m \hat{R}_m(t) \otimes \hat{T}_m, \quad (1)$$

where \hat{T}_m shifts the walker by m lattice sites, and $\hat{R}_m(t) = \vec{r}_m(t) \cdot \vec{\sigma}$ rotates its spin. Here and in the following $\vec{\sigma} = (\sigma_0, i\vec{\sigma})$ and $\vec{r}_m = (r_{m0}, \mathbf{r}_m)$ are four component vectors such that $\sigma_0 = \mathbb{1}_2$, $\vec{\sigma} = (\sigma_x, \sigma_y, \sigma_z)$ and $\vec{r}_m \in \mathbb{C}^4$. Central for our proposal is the time-dependent spin rotation axes $\mathbf{r}_m(t)$ which are dynamically changed in the course of the walk. As we show below, using dynamical protocols with periods that are incommensurate with the

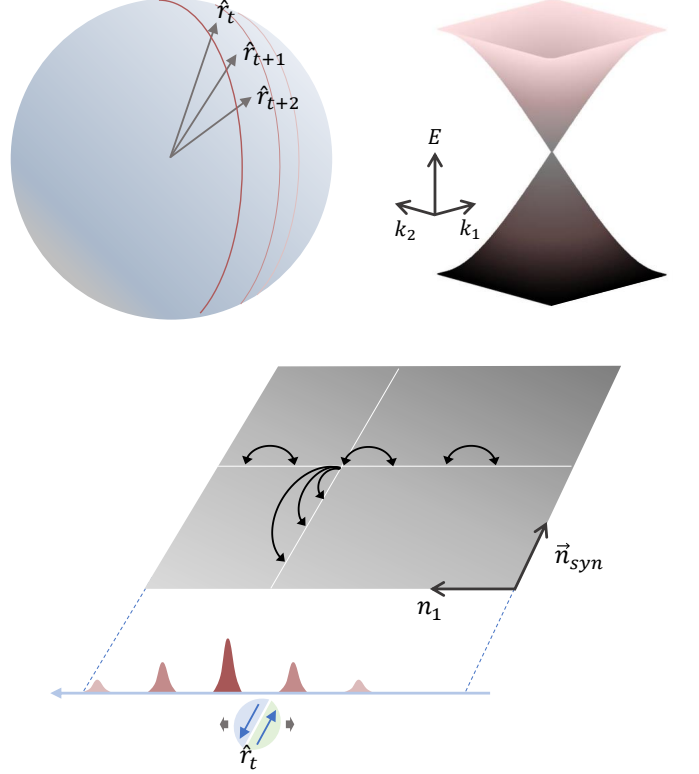


FIG. 1. A $1d$ quantum walk with time-dependent spin quantization axis \hat{r}_t can simulate dynamics of a $2d$ systems when the period of r_t is incommensurate with the discrete time-steps of the evolution operator. This engineering of synthetic dimensions allows to sidestep the fermion doubling principle, and to simulate e.g. the $2d$ surface states in isolation of a $3d$ quantum spin Hall insulator.

discrete time step of the evolution operator Eq. (1) enables the simulation of dynamics in higher dimensional systems. In the following we will focus on quantum walks with short-range hops to the nearest neighbors, $m \in \{0, -1, +1\}$. The unitary operator Eq. (1) then simplifies to

$$\hat{U}_t = \vec{r}_0 \cdot \vec{\sigma} + (\vec{r}_+ \cdot \vec{\sigma}) \otimes \hat{T}_+ + (\vec{r}_- \cdot \vec{\sigma}) \otimes \hat{T}_-, \quad (2)$$

and unitarity sets the following constraint on \vec{r}_0, \vec{r}_\pm : Expressing $\vec{r}_\pm = \vec{r}_r \pm i\vec{r}_i$, with $\vec{r}_{r,i} \in \mathbb{R}^4$ real four component vectors, the latter are orthogonal, $\vec{r}_r \cdot \vec{r}_i = 0$, $\vec{r}_0 \cdot \vec{r}_{r,i} = 0$, and equal in magnitude, $|\vec{r}_r| = |\vec{r}_i| = \frac{1}{2}\sqrt{1 - |\vec{r}_0|^2}$ at each time step t (see Appendix A for details).

Finally, we add spin-dependent spatial disorder to the dynamics. To this end we introduce the unitary matrix $(\hat{U}_{\text{dis}})_{nn'} = \hat{U}_{\text{dis}}(n)\delta_{nn'}$ where $\hat{U}_{\text{dis}}(n)$ are independent random spin rotation matrices, acting locally on each site n . The single time-step evolution $|\psi_t\rangle = \mathcal{U}_{t,t-1}|\psi_{t-1}\rangle$ generating the $1d$ quantum walk is then composed of the combined operator,

$$\mathcal{U}_{t,t-1} = \hat{U}_t \hat{U}_{\text{dis}}, \quad (3)$$

and we next discuss its potential to simulate higher dimensional dynamics.

A. Synthetic dimensions from multi-frequency dynamical protocols

Let us specify the protocol Eq. (1) to rotations \hat{R}_m which depend on d_{syn} time-dependent functions,

$$\hat{R}_m(t) \equiv \hat{R}_m(\varphi_{2,t}, \dots, \varphi_{d_{\text{syn}}+1,t}), \quad (4)$$

and where the time-dependence for each of the functions is of the form $\varphi_{i,t} = k_i + \omega_i t$ with frequencies $\omega_2, \dots, \omega_{d_{\text{syn}}+1}$ incommensurate to 2π and among themselves. Further, $k_{\text{syn}} \equiv (k_2, \dots, k_{d_{\text{syn}}+1})$ are arbitrary initial phases which we consider averaged over in our dynamical protocols below. The mapping to an effectively $1 + d_{\text{syn}}$ dimensional Floquet system is achieved by extending the Hilbert space of the system and interpreting these phases as momenta conjugate to integer valued coordinates $n_{\text{syn}} = (n_2, \dots, n_{d_{\text{syn}}+1})$, with canonical commutation relations $[\hat{n}_i, \hat{k}_j] = -i\delta_{ij}$ between the corresponding operators. We note that $\hat{n}_i = -i\partial_{k_i}$ in the phase-momentum representation of the theory. These coordinates extend the lattice in $1 + d_{\text{syn}}$ dimensions with sites $\mathbf{n} = (n_1, n_{\text{syn}})$, where $n_1 = n$ is the physical lattice coordinate, conjugate to a phase k_1 . In the same notation, $\mathbf{k} = (k_1, k_{\text{syn}})$.

Using the general relation $e^{ia\hat{n}} f(\hat{k}) e^{-ia\hat{n}} = f(\hat{k} + a)$, the time dependence in the arguments of the rotation operator can be removed by the gauge transformation

$$\hat{R}_m(t) = e^{i\omega_j t \hat{n}_j} R_m(0) e^{-i\omega_j t \hat{n}_j}, \quad (5)$$

where a summation over $j = 2, \dots, 1 + d_{\text{syn}}$ is implicit. This enables us to express the time evolution operator $\mathcal{U}_{t,0} \equiv \mathcal{U}_{t,0} \equiv \prod_{\tau=0}^{t-1} \mathcal{U}_{\tau+1,\tau}$ as

$$\begin{aligned} |\psi_t\rangle &= \mathcal{U}_{t,t-1} \mathcal{U}_{t-1,t-2} \dots \mathcal{U}_{1,0} |\psi_0\rangle \\ &= e^{i\omega_j t \hat{n}_j} [\mathcal{U}_{0,-1} e^{-i\omega_j \hat{n}_j}]^t |\psi_0\rangle. \end{aligned} \quad (6)$$

We notice that the time evolution is governed by powers of the single *Floquet operator* $\mathcal{U}_F \equiv \mathcal{U}_{0,-1} e^{-i\omega_j \hat{n}_j} = \hat{U}_{t=0} \hat{U}_{\text{dis}} e^{-i\omega_j \hat{n}_j} \equiv U_{\mathbf{k}} \hat{W}_{\mathbf{n}}$. Here, $\hat{W}_{\mathbf{n}} \equiv \hat{U}_{\text{dis}}(n_1) e^{-i\omega_j \hat{n}_j}$ is diagonal in the coordinate representation, while $\hat{U}_{\mathbf{k}} = \hat{U}_0(\mathbf{k})$ is momentum-diagonal. To understand this last statement, we note that in Eq. (1) the coordinate translation operator $\hat{T}_m f(n_1) = f(n_1 - m)$ affords the representation $\hat{T}_m = e^{im\hat{k}_1}$ while $\hat{R}_m(0)$ depends on the phases k_{syn} .

To summarize, our dynamics is governed by the effective multi-dimensional Floquet operator $\mathcal{U}_F = \hat{U}_{\mathbf{k}} \hat{W}_{\mathbf{n}}$ factoring into two pieces which are individually diagonal in coordinates and momenta, respectively. Our numerical simulations below demonstrate that the combined action of these operators induces integrability breaking, physically equivalent to static disorder, in all $1 + d_{\text{syn}}$

dimensions. However, before introducing quantum simulators for the combined effects of disorder and topology in this setting, we briefly introduce observables probing topological surface states in an experimentally accessible way.

B. Observable

The spreading after t time steps of a wave packet, describing a quantum walker initially prepared at site $n_1 = 0$ with spin σ , can be expressed as

$$\langle \Delta X^2 \rangle \equiv \sum_{n_1} \sum_{\sigma', \sigma} n_1^2 |\overline{\langle n_1, \sigma' | \mathcal{U}_{t,0} | 0, \sigma \rangle}|^2. \quad (7)$$

Here the sum is over spin orientations $\sigma = \uparrow, \downarrow$ and $\overline{(\dots)}$ refers to the average over both, an ensemble of realizations of the random rotations \hat{U}_{dis} and the initial momenta k_{syn} . In a mixed coordinate-momentum representation, basis states of the extended Hilbert space are defined by the kets $|n_1, \sigma\rangle \rightarrow |n_1, k_{\text{syn}}, \sigma\rangle$. Specifically, the initial state of the quantum walker is confined to $n_1 = 0$, and independent of synthetic momenta. Upon Fourier transformation to a full coordinate representation, $|n_1, k_{\text{syn}}, \sigma\rangle \rightarrow |n_1, n_{\text{syn}}, \sigma\rangle \equiv |\mathbf{n}, \sigma\rangle$ this translates to localization at $|0, \sigma\rangle$ in both physical and synthetic space. The spreading of the quantum walker is thus given by (see further details in Appendix B)

$$\langle \Delta X^2 \rangle \equiv \sum_{\mathbf{n}} \sum_{\sigma', \sigma} n_1^2 |\overline{\langle \mathbf{n}, \sigma' | \mathcal{U}_F^t | 0, \sigma \rangle}|^2. \quad (8)$$

The correlation function Eq. (8) describes the width in the physical n_1 -direction of the wave packet initially prepared at $n_1 = 0$, and its finite time scaling encodes information on the quantum walk dynamics.

C. Topological invariants

All our topological FMs to be discussed below are characterized by integer valued invariants. These numbers afford two different interpretations:

Topological invariants and FM classification: The first relates to a classification of FM phases in terms of the periodic table of Hamiltonian insulators[3]. Its idea is to map the translation-invariant part of the Floquet operator $U_{\mathbf{k}}$ onto a block off-diagonal ‘auxiliary’ Hamiltonian

$$H_{\mathbf{k}} = \begin{pmatrix} & U_{\mathbf{k}} \\ U_{\mathbf{k}}^\dagger & \end{pmatrix}. \quad (9)$$

This Hamiltonian inherits the symmetries of $U_{\mathbf{k}}$, but in addition possesses a ‘chiral’ symmetry due to its off-diagonality; it belongs to a symmetry class different from the class of the Floquet theory. For example, if the latter is in class A (just unitary), H will be in class AIII

(chiral, no further symmetries.) Bott periodicity then implies that a class A Floquet theory realizes a FM state in odd effective dimension $D = d + d_{\text{syn}}$ if the associated D -dimensional Hamiltonian in class AIII is also topologically non trivial. Further, the presence of topologically non trivial phases of the Hamiltonian theory is signaled by invariants mathematically identical to those constructible for the Floquet theory. For example, in the above case, these invariants are ‘winding numbers’ defined by a unitary map from odd-dimensional Brillouin zones $\mathbf{k} \mapsto U_{\mathbf{k}}$ into the unitary group. These winding numbers classify class AIII insulating phases in odd dimensions and class A Floquet metallic phases in even dimensions.

Topological invariants and localization theory: To understand this statement in more concrete terms, we note that our Floquet theories are categorically disordered or chaotic. Their physical description requires real space methods, as defined by the nonlinear σ -models of disordered conductors. In these theories protection against the effects of Anderson localization, i.e. topological metallicity, is introduced via topological terms (see Eq.(25) for a concrete example). These terms take physical effect provided their coupling constants are not vanishing. Below, we will demonstrate in two concrete case studies that the momentum space invariants responsible for the ‘abstract’ classification of topological FMs indeed feature as coupling constants in the topological field theories. In this way, they serve a double function in the classification and the localization theory of FMs. In the latter context, they protect topological FMs from developing a ‘mobility gap’ and force them to remain metallic, including FMs in low dimensions which would otherwise show strong localization.

III. THREE DIMENSIONAL TOPOLOGICAL FLOQUET METAL FM_{1+2_{syn}}

The concept of synthetic dimensions is general and can be realized for a wide class of driven or kicked Floquet systems [16, 19–22]. In the following, we introduce a specific realization in $1 + 2_{\text{syn}}$ dimensions, physically equivalent to the surface of a four dimensional topological insulator in symmetry class A (aka ‘four-dimensional quantum Hall insulator’).

A. Model

We consider a one dimensional quantum walker, whose forward and backward hopping amplitudes are time-dependent matrices coupling to the internal degrees of freedom (see Fig. 1). In the notation of the previous section, its time evolution from one discrete time step, t , to the next is defined through

$$\hat{U}_t = \frac{1}{2}(\sigma_0 + \mathbf{r}_t \cdot \boldsymbol{\sigma}) \otimes \hat{T}_+ + \frac{1}{2}(\sigma_0 - \mathbf{r}_t \cdot \boldsymbol{\sigma}) \otimes \hat{T}_-, \quad (10)$$

where the specific choice

$$\mathbf{r}_t = (\cos \varphi_{2,t} \sin \varphi_{3,t}, \sin \varphi_{2,t} |\sin \varphi_{3,t}|, \cos \varphi_{3,t}), \quad (11)$$

will be motivated momentarily, and the time dependence of the phase arguments is defined below Eq.(4). Turning to the gauge-equivalent representation in terms of a Floquet operator acting in a space with one physical and two synthetic dimensions, we describe the dynamics through the Floquet operator $\hat{U}_F = \hat{U} \hat{W}_{\mathbf{n}}$ with $U_{\mathbf{k}} = U_{t=0}$ and $\hat{T}_{\pm} = e^{\pm i k_1}$. For later reference, we note that the unitary $U_{\mathbf{k}}$ affords different representations, each useful in its own right. First, it is straightforward to verify that

$$\begin{aligned} \hat{U}_{\mathbf{k}} &= \exp [i k_1 (\mathbf{r}(\mathbf{k}) \cdot \boldsymbol{\sigma})], \\ \mathbf{r}(k) &= (\cos k_2 \sin k_3, \sin k_2 |\sin k_3|, \cos k_3). \end{aligned} \quad (12)$$

Alternatively, we may represent the spin matrices as rotations acting upon a translation operator with z -axis polarization: $\hat{U}_{\mathbf{k}} = R_3(-k'_2) R_2(-k_3) \hat{T}_C R_2(k_3) R_3(k'_2)$ with $\hat{T}_C = e^{i k_1 \sigma_3}$, the momentum $k'_2 = k_2 \text{sgn } k_3$, and spin rotation operators $R_j(\varphi_l) = \exp(i \varphi_l \sigma_j / 2)$.

A crucial feature of this realization is its non-analytic dependence on the momentum variables through $|\sin k_3|$. In the Fourier conjugate representation it translates to long ranged hopping $(\mathcal{U}_F)_{n_3 n'_3} \sim |n_3 - n'_3|^{-2}$ [23]. At this point, the synthetic dimensions begin to play an essential role: power law hopping in physical dimensions is difficult to engineer. More importantly, the $|\sin k_3|$ non-analyticity is the essential resource allowing us to sidestep the fermion doubling theorem and to realize a synthetic topological metal.

Winding number:—To elucidate this last point, we interpret Eq. (12) as a mapping from the $3d$ Brillouin zone torus to the two-dimensional special unitary group $\mathbb{T}^3 \rightarrow \text{SU}(2)$ (with unit determinant, $\det[U_{\mathbf{k}}] = 1$), and assign the topological invariant

$$\begin{aligned} W &= \frac{1}{24\pi^2} \int d^3 \mathbf{k} \epsilon^{\mu\nu\rho} \text{tr} \left[(U_{\mathbf{k}}^\dagger \partial_\mu U_{\mathbf{k}}) (U_{\mathbf{k}}^\dagger \partial_\nu U_{\mathbf{k}}) (U_{\mathbf{k}}^\dagger \partial_\rho U_{\mathbf{k}}) \right] \\ &= \frac{1}{2\pi^2} \int d^3 \mathbf{k} \sin^2 k_1 |\sin k_3| = 4, \end{aligned} \quad (13)$$

where $\mu, \nu, \rho \in \{1, 2, 3\}$. As anticipated above, it is the non-analyticity $|\sin k_3|$ that leads to a non-vanishing winding number. Conversely, a model with analytic k -dependence would necessarily lead to a vanishing winding number, in accordance with the fermion doubling theorem.

Driving protocols with non-analytic functions, simulating power law hoppings in synthetic space, allow to construct Floquet operators with even winding numbers $W \in 2\mathbb{Z}$: The starting point of our construction are realizations of unitary operators which display finite winding numbers over certain subsets of a Brillouin zone, say $W = n$ in region I and $W = -n$ in region II. (The numbers must add to zero by virtue of the fermion doubling theorem.) The trick to generate a finite winding number then is to modify the momentum dependence in region II

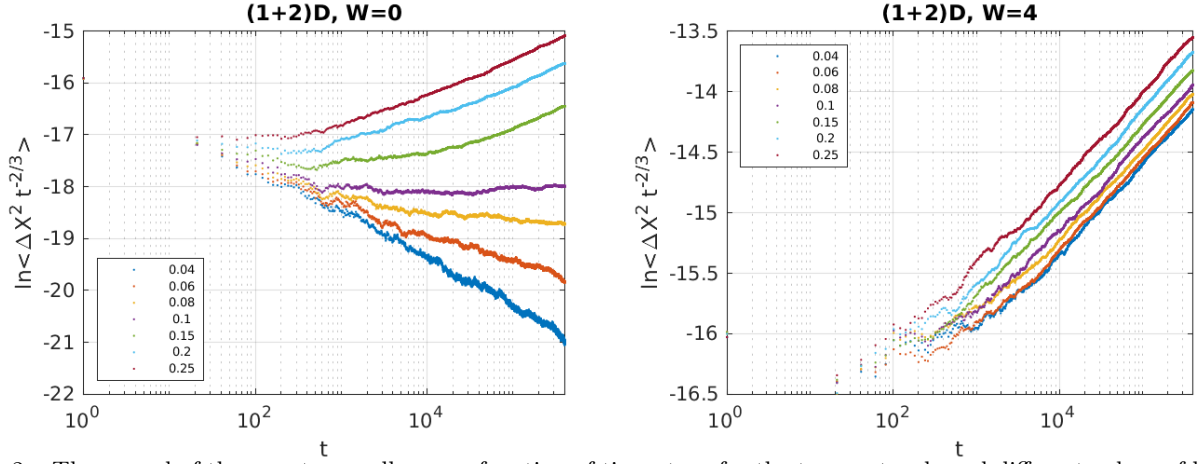


FIG. 2. The spread of the quantum walker as a function of time steps for the two protocols and different values of bandwidth w introduced in Eq. (14). To facilitate observation of the metal-to-insulator transition, the width of wave packet is rescaled by the critical scaling at the transition, $\langle \Delta X^2 \rangle \sim t^{2/3}$. Left panel: The topologically trivial protocol, $W = 0$, shows a metal-to-insulator transition for $w \simeq 0.1$. Right panel: The topological non trivial variant, $W = 4$, shows no signatures of localization, i.e. $\langle \Delta X^2 \rangle \sim t$ for all values w and up to $t \sim 5 \times 10^5$ time steps.

via a sign change in the momentum dependence which inverts the winding number to $W|II = +n$ and $W = 2n$ in total. We also constructed an alternative model with the minimal winding possible in this scheme, $W = 2$. Since it was rather involved we opted, however, for the discussion of the simpler $W = 4$ variant, Eqs. (10) and (11). We also emphasize that winding numbers for topological Floquet systems cannot be simply understood from their low energy effective Hamiltonians [24]. $W = 4$ of Eq. (12) is e.g. not related to four Weyl cones in a low energy description, but rather stores information on the entire Brillouin zone (see also discussion on dispersion of Eq. (12) in the next subsection).

The invariant Eq.(13) indicates topological metallicity of our Floquet system. Within the alternative interpretation discussed above, the non-vanishing winding number, W , signals topological non-triviality of the ‘auxiliary’ class AIII Hamiltonian. Bott periodicity implies non trivial phases of $4d$ class A systems (the four-dimensional quantum Hall effect), and the original Floquet system describes the physics of its three dimensional metallic surface state. In more concrete terms, we will see in section V that the winding number W features as a building block in our construction of a gapless effective field theory equivalent to that of a three-dimensional topological metal.

B. Numerical simulations

To independently verify the topological metallic nature of the $3d$ dynamics simulated by the protocol Eq. (10) we have run numerical simulations. More specifically, we have simulated the quantum walk with trivial and non trivial winding numbers for varying effective disorder strengths by introducing additional bandwidths in

the model, as we discuss next. This allows to test our main prediction, that is, the absence of Anderson localization for all disorder strength for finite windings W , contrasting Anderson localization at large disorder for vanishing winding number $W = 0$.

Simulation details:—We numerically study the time evolution of an initially localized wave packets, under influence of the $1d$ quantum walk operator Eq. (10). To allow for a comparison of topologically trivial and non trivial quantum walks with same energy-momentum dispersion relation of the clean system, we implement the walk with $|\sin \varphi_{3,t}|$, as indicated in Eq. (12), and a second protocol with $|\sin \varphi_{3,t}|$ replaced by $\sin \varphi_{3,t}$. A metal-to-insulator transition with increasing disorder strength is expected for the second protocol. The static spatial disorder \hat{U}_{dis} is implemented by randomly drawing spin rotation matrices from the uniform Haar measure. That is, the disorder strength is fixed and we need to introduce some tunable parameter allowing to drive a (possible) metal-to-insulator transition. We then notice that Eq. (12) and its topologically trivial cousin have no energy dispersion in $k_{2,3}$ direction, which makes the latter always prone to localization. At the same time, we can perturb the original models to generate a dispersion with tunable bandwidth w in $k_{2,3}$ -direction. This then allows to study a delocalization transition as a function of w . To realize this idea, we multiply the original single time-step evolution operators by the unitary operator

$$\hat{U}_w = \exp[iw(\sin k_{2,t}\sigma_1 + \sin k_{3,t}\sigma_2)], \quad (14)$$

which does the job. We then study the time scaling of the average spread $\langle \Delta X^2 \rangle$ of the initial wave packet in the physical dimension.

Results:—Fig. 2 shows the time evolution of $\langle \Delta X^2 \rangle$ for the two protocols and different values of the bandwidth w , as indicated in the legend. The vertical axis is

rescaled by the time-dependence $\langle \Delta X^2 \rangle \sim t^{2/3}$ expected at the metal-to-insulator transition [5]. For the trivial protocol $W = 0$ (left panel) one clearly sees the metallic ($w > 0.1$) and insulating ($w < 0.1$) regimes separated by critical scaling at $w \simeq 0.1$. In contrast, the topological non trivial protocol with $W = 4$ (right panel) shows metallic behavior for all values of w , with $\langle \Delta X^2 \rangle \sim t$ up to the largest time steps 5×10^5 . The two incommensurate frequencies here were chosen as $\omega_2 = 2.4\sqrt{5}$, $\omega_3 = 2.4\sqrt{15}$, and disorder averaging is over 50 realizations for each data point. We also notice that the long-time numerical results are independent of the specific value for the incommensurate frequencies.

In case of the trivial protocol $W = 0$, deviations from classical scaling $\langle \Delta X^2 \rangle \sim t$ signals Anderson localization, and eventually the dynamics will entirely freeze, $\langle \Delta X^2 \rangle \sim t^0$, on longer time and length scales. The important observation for us is that a clear distinction between quantum simulators of trivial and topological metallic phases are noticeable already for a small number of $\mathcal{O}(20)$ time steps, see Fig. 3(c) and (d). This is crucial, once it comes to an experimental implementation of the quantum walks, as we discuss next.

C. Experimental realization: A $\text{FM}_{1+2_{\text{syn}}}$ simulator

So far we have shown how the freedom of choosing operators of arbitrary k -dependence in the synthetic momentum space allows for the engineering of topological Floquet operators that cannot exist in autonomous lattice environments. Specifically, we have (i) proposed a concrete dynamical protocol based on a $1d$ quantum walk, (ii) shown that this simulates a topological metal e.g. realized on the isolated surface of a $4d$ quantum Hall insulator, and (iii) demonstrated that its most characteristic feature—absence of Anderson localization at strong disorder—can be observed already after $\mathcal{O}(20)$ time steps. The final piece of our proposal is to indicate an experimental platform that offers the required flexibility to implement dynamical protocols for spin-1/2 walkers. We here argue that linear optical networks are ideally suited to realize the proposed quantum simulators. After a brief review of their principal elements, we suggest a blueprint for the quantum Hall simulator.

Principle elements:—In the typical optical realization of a quantum walk, photons propagate through a network of linear elements, viz. beam splitters, phase shifters and polarization plates, realizing the “step” and “coin” operations. The step operation typically implements chiral hopping (here as a matrix in spin space)

$$\hat{T}_C \equiv \begin{pmatrix} \hat{T}_+ & \\ & \hat{T}_- \end{pmatrix}, \quad (15)$$

translating the walker to the right (T_+) or (T_-) left according to its spin being in the up (first component), respectively, down state (second component). The dy-

namical coin operations realize spin rotations, $\hat{R}(t)$. Using an Euler angle decomposition they can be generated from repeated application of elementary rotations around any two of the three internal axes

$$\hat{R}_j(\varphi_{l,t}) = \exp(i\varphi_{l,t}\sigma_j/2), \quad j = y, z, \quad l = 2, 3, \quad (16)$$

with Pauli matrices operating in spin space. The great flexibility offered by optical linear networks is that Euler angles $\varphi_{l,t} = k_l + \omega_l t$ can be changed dynamically during the realization of the quantum walk.

The successive application of chiral step and coin operations composing the quantum walk protocol is implemented in a “feedback loop”, see Fig. 3(b). Typically, a coherent laser pulse attenuated to an average single-photon per pulse injects photons into the linear network. Horizontal and vertical polarizations of the photon constitute the internal “spin”-states. The step operation \hat{T}_C is realized in time, employing a polarizing beam splitter in combination with fiber delay lines. That is, horizontally and vertically polarized photons are separated by the beam splitter and send through fiber lines of different lengths. The length mismatch of the fibers introduces a well-defined delay between the two polarization components. When coherently recombined, the temporal separation of the two components is equivalent to the spatial separation by two lattice sites induced by the chiral translation to left and right neighbors of the $1d$ lattice. Dynamical coin operations $\hat{R}_j(\varphi_{l,t})$ are realized via tunable polarization rotations. In practice, the dynamical control over only one rotation-axis, e.g. the z -axis is required, and rotations around remaining axes are realized by the combination with suitable polarization controllers, i.e. half- and quarter-wave plates [25].

The dynamical control is achieved via control voltages applied to fast-switching electro-optic modulators (EOMs) that change rotation-angles on time scales shorter than a step operation. Recent progress allows to operate the latter without high additional losses and walks up to $t = 30 - 40$ time-steps have been reported within this set up, see e.g. Refs. [8, 18]. From the numerical simulations of the previous section, we expect this to be sufficient to distinguish the dynamics of a topological from a trivial Floquet metal. After the light pulses have been fed back into the loop of step and coin operations, realizing a single time step operation, for the desired number of time steps they are released to the detection unit, see Fig. 3(b). Repeating the procedure for varying numbers of time-steps and different realizations of coin operations, one obtains the walker’s probability distribution which allows for the full characterization of its dynamics.

Blueprint for the $\text{FM}_{1+2_{\text{syn}}}$:—A detailed blueprint for an optical linear network simulating the topological $\text{FM}_{1+2_{\text{syn}}}$ is shown in Fig. 3. A crucial observation here is that the chiral translational U_t (10) with tunable spin-quantization axis \mathbf{r}_t can be implemented via a step operation T_C dressed by coin operations, $\hat{U}_t = \hat{R}_t^\dagger \hat{T}_C \hat{R}_t$, with the coin matrix \hat{R}_t being a product of two elementary

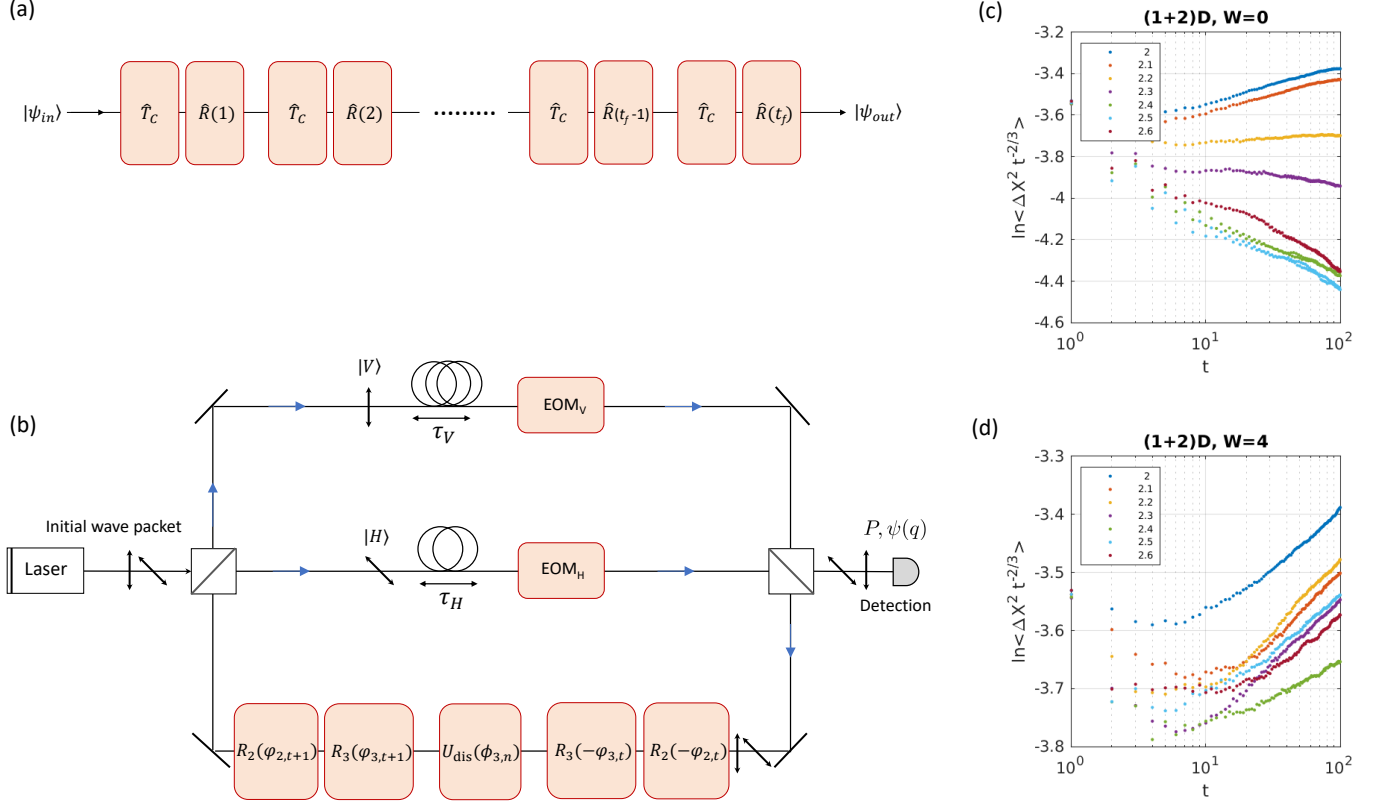


FIG. 3. (a,b) Blueprint of an optical linear network simulating the topological surface states of a $4d$ quantum Hall insulator in the quantum walk setting. The feedback loop is build of the step operator \hat{T}_C (upper and middle arms) followed by the coin operator $\hat{R}(t) = R_{t+1}\hat{U}_{\text{dis}}R_t^\dagger$ (lower arm), for details see main text. To the left and right of the loop, source and detection units are connected. The source consist of a laser and a polarizing beam splitter (PBS) that allows for the preparation of the initial state. The passage to the detection unit can be activated by the dynamically tunable EOMs following the fiber lines of the step operation. In the detection unit photons are registered by avalanche photo-diode (APD). (c,d) Numerical simulations of wave packet spreading for trivial and topological quantum walks, here for varying incommensurate frequencies. The latter are chosen as $\omega_2 = C\sqrt{5}$ and $\omega_3 = C\sqrt{15}$ for several values $2.0 \leq C \leq 2.6$ (see legends). Differences between the two systems become visible already after $t \gtrsim 10$ time steps: the topological metal (d) shows robust diffusion for all values of C , while a crossover from diffusive to subdiffusive dynamics is observed as $C > 2.4$ for the trivial metal (c).

rotations, $\hat{R}_t = \hat{R}_y(\varphi_{3,t})\hat{R}_z(\varphi_{2,t})$, where

$$\varphi_{3,t} = k_3 + \omega_3 t, \quad (17)$$

$$\varphi_{2,t} = \begin{cases} k_2 + \omega_2 t, & \sin(\varphi_{3,t}) \geq 0, \\ -k_2 - \omega_2 t, & \sin(\varphi_{3,t}) < 0, \end{cases} \quad (18)$$

(note the conditional value of $\varphi_{2,t}$ depending on the sign of $\sin(\varphi_{3,t})$, which follows from the definition (11) of the vector \mathbf{r}_t). The role of \hat{R}_t is to rotate \mathbf{z} -axis into the instantaneous spin quantization axis \mathbf{r}_t .

In the linear network set-up it is convenient to start the feedback loop with a step operation. Reorganizing thus spin rotations and the local disorder potential in the originally defined one step evolution operator $\mathcal{U}_{t,t-1} = \hat{U}_t \hat{U}_{\text{dis}}$ (with \hat{U}_{dis} specified below), we construct the equivalent one as the following succession of step and coin opera-

tions,

$$\mathcal{U}_{t+1,t} = \hat{R}(t)\hat{T}_C, \quad \hat{R}(t) = \hat{R}_{t+1}\hat{U}_{\text{dis}}\hat{R}_t^\dagger. \quad (19)$$

This sequence is then iterated for the desired number of time steps.

Fig. 3(a) schematically shows the elements of quantum walk operations to be applied to an initial localized wave packet before the detection after t_f time steps. The actual implementation of the linear optical network can be prepared as in Fig. 3(b), realizing chiral quantum walk and coin operators. The $\text{EOM}_{V,H}$ are equipped for the initiation and the readout of the quantum walk simulation. For the static disorder in real space, we suggest to follow the protocol used in the numerical simulations with fixed bandwidth. That is, choosing $\hat{U}_{\text{dis}} = R_z(\phi_{n_1})$ with static local angles ϕ_{n_1} , randomly drawn from the

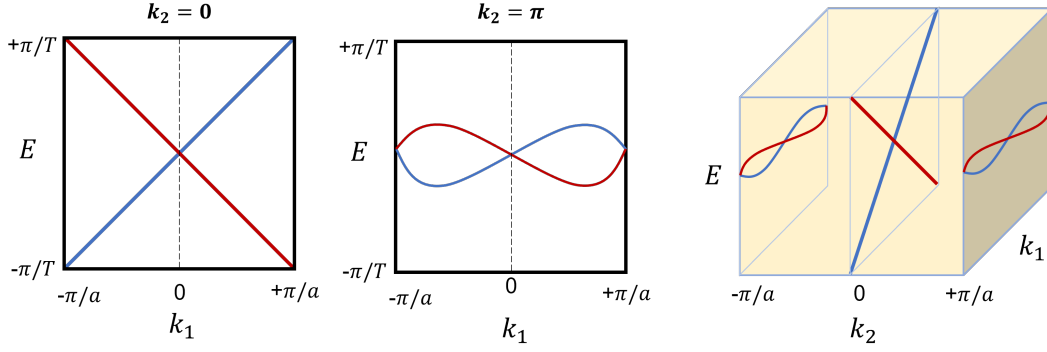


FIG. 4. Dispersion relations of the quasi-energy spectrum of the two-band model along the high symmetry lines $k_2 = 0$ (left) and $k_2 = \pi$ (middle), respectively, see also discussion in the main text. The former contributes to the topological invariant by the factor $\text{Pf}[w_{\Lambda_1}] \text{Pf}[w_{\Lambda_2}] = -1$, while the latter gives the factor $\text{Pf}[w_{\Lambda_3}] \text{Pf}[w_{\Lambda_4}] = 1$. Here $w_{\mathbf{k}}$ is the antisymmetric sewing matrix. Right panel: Visualization of dispersions along the high-symmetry lines in the 2d Brillouin zone.

unit circle $-\pi \leq \phi_{n_1} < \pi$, and frequencies ω_2, ω_3 indicated in the previous section.

Fig. 3(c) and (d) shows numerical results for the quantum simulators of the trivial ($W = 0$) and topological ($W = 4$) metal over a range of experimentally accessible time steps. Here the bandwidth is set to $w = 0$, and incommensurate frequencies are varied as $\omega_2 = C\sqrt{5}, \omega_3 = C\sqrt{15}$ with values of C indicated in the legend. There are notable differences between the two systems already after $t \gtrsim 10$ time steps: Dynamics for the topological metal is diffusive for all values of C , while the trivial system shows a C -dependent behavior reminiscent of a metal-insulator transition as C is increased. Notice, however, that the metallic behavior for small values $C = 2, 2.1$ only holds for short time, and localization sets in at longer times (i.e. for the trivial protocol there is no true metallic phase at $w = 0$, as discussed above).

This finalizes our discussion of a quantum simulator for the surface states of a 4d quantum Hall insulator. We next discuss generalizations to other dimensions and symmetry classes.

IV. TWO DIMENSIONAL FLOQUET TOPOLOGICAL METAL $FM_{1+1\text{syn}}$

To illustrate the generality of our approach, we next discuss the example of a quantum simulator for surface states in a symmetry class different from the quantum Hall insulators. Specifically, we propose a simulator for the 2d surface states of a class AII quantum spin Hall insulator in $d = 3$.

To this end, we start out from a 1d quantum walk, Eq. (2), with dynamical protocol,

$$\begin{aligned} \vec{r}_0 &= \frac{1}{2}(1 - \cos \varphi_{2,t}, 0, 0, \sin \varphi_{2,t}), \\ \vec{r}_r &= \frac{1}{4}(-1 - \cos \varphi_{2,t}, 0, 0, \sin \varphi_{2,t}), \\ \vec{r}_i &= \frac{1}{4}(0, |\sin \varphi_{2,t}|, -1 - \cos \varphi_{2,t}, 0), \end{aligned} \quad (20)$$

where $\varphi_{2,t} = k_2 + \omega_2 t$ and the frequency ω_2 incommensurate to 2π . The three vectors Eq. (20) are orthogonal to each other, and unitarity of the single time-step evolution operator follows from $|\vec{r}_0| = |\sin \varphi_{2,t}/2|$ and $|\vec{r}_{r,i}| = \frac{1}{2}|\cos \varphi_{2,t}/2|$, see also Appendix A. Upon Fourier transform in the physical coordinate and gauge transformation to eliminate time dependence of the driving protocol, we arrive at the Floquet operator

$$\hat{U}_{\mathbf{k}} = (\hat{r}_0 \cdot \vec{\sigma}) + (\vec{r}_+ \cdot \vec{\sigma})e^{ik_1} + (\vec{r}_- \cdot \vec{\sigma})e^{-ik_1}, \quad (21)$$

where $k_2 = \varphi_{2,t=0}$ and $\vec{r}_{\pm} = (\vec{r}_r \pm i\vec{r}_i)$. We notice that the specific choice of the driving protocol has lead to the non-analytical n_2 -component $\propto |\sin k_2|$. It is again this unusual dependence, impossible to realize on a lattice with finite range hopping, which allows us to sidestep the fermion doubling theorem. It is readily verified that Eq. (21) satisfies the time reversal relation $\sigma_2 \hat{U}_{\mathbf{k}}^T \sigma_2 = \hat{U}_{-\mathbf{k}}$ of class AII systems. The latter host topological insulating \mathbb{Z}_2 phases in 3d, and thus topological metallic Floquet phases in 2d.

A. Topological invariant

To demonstrate the topological nature of the protocol Eq. (20), we focus on the translational invariant part $U_{\mathbf{k}}$, and consider the latter as a map from the 2d Brillouin zone torus to the special unitary group $\mathbb{T}^2 \rightarrow \text{SU}(2)$ ($\det[\hat{U}_{\mathbf{k}}] = 1$). Time reversal symmetry imposes that $n(\mathbf{k}) \parallel e_0$ at the four time-reversal invariant momenta, $\Lambda_1 = (0, 0)$, $\Lambda_2 = (0, \pi)$, $\Lambda_3 = (\pi, 0)$, and $\Lambda_4 = (\pi, \pi)$. At these points the so-called sewing matrix $w_{\mathbf{k}} = -i\sigma_2 \hat{U}_{\mathbf{k}}^T$ is anti-symmetric and the map $\hat{U}_{\mathbf{k}}$ is thus characterized by the \mathbb{Z}_2 topological index,

$$W_{\mathbb{Z}_2} = \prod_{i=1}^4 \text{Pf}[-i\sigma_2 \hat{U}_{\Lambda_i}^T] = -1, \quad (22)$$

where in the last identity we used that for Eq. (21) $\hat{U}_{\Lambda_1} = \sigma_0$, while $\hat{U}_{\Lambda_i} = -\sigma_0$ for $i = 2, 3, 4$. Notice that the non-

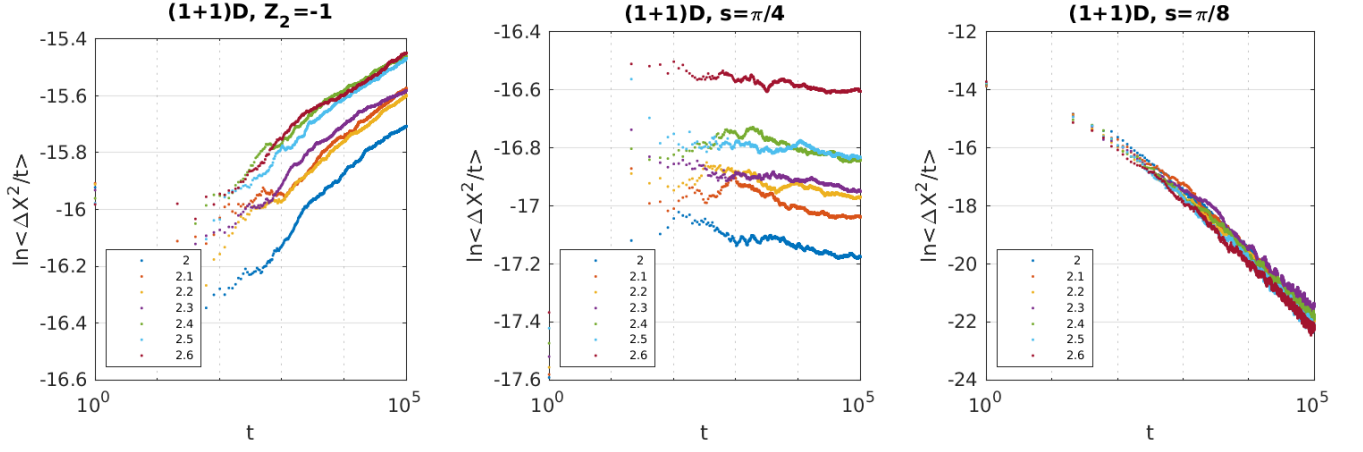


FIG. 5. The scaled width of a wave packet $\langle \Delta X^2 \rangle / t$ for different quantum walks in $(1+1_{syn})D$ and monitored over 5×10^5 time steps. (Left) Topological quantum walk showing anomalous super diffusion, (middle) critical quantum walk of a class A model fine tuned to a topological phase transition, (right) topologically trivial quantum walk subject to Anderson localization. Colors correspond to incommensurate frequencies $\omega_2 = \sqrt{5}C$ with values C indicated in the legend.

triviality of the index follows from the specific choice of the n_2 -component.

Building on the alternative interpretation of the topological invariant discussed earlier, $W_{\mathbb{Z}_2}$ signals topological non-triviality of its auxiliary class DIII Hamiltonian [3]. Indeed, time-reversal symmetry of the latter is inherited from the Floquet operator, while block off-diagonal structure induces the additional chiral structure. In this interpretation Eq. (22) then encodes topological properties of the class DIII system in $2d$ [26].

For a more intuitive interpretation of Eq. (22), we prove in Appendix D that the Pfaffians can be expressed as $\text{Pf}(w_{\Lambda_j}) = -\exp(i\epsilon_{\Lambda_j})$, where ϵ_{Λ_j} are the quasi-energies of $U_{\mathbf{k}}$ at the time-reversal invariant momenta Λ_j . The \mathbb{Z}_2 topological invariant thus affords the alternative representation

$$W_{\mathbb{Z}_2} = \exp\left(i \sum_{j=1}^4 \epsilon_{\Lambda_j}\right), \quad (23)$$

which has a simple intuitive visualization. To this end, consider the $1d$ dispersion relations $E_{\pm}^0(k_1) = \epsilon_{\pm}(k_1, k_2 = 0)$ and $E_{\pm}^{\pi}(k_1) = \epsilon_{\pm}(k_1, k_2 = \pi)$ of the quasi-energy spectrum $\epsilon_{\pm}(\mathbf{k})$ of the two-band model along the two high symmetry lines $k_2 = 0, \pi$, respectively. As shown in Fig. 4, bands $E_{\pm}^0(k_1)$ touch at Λ_1 and are split by energy 2π at Λ_2 . Bands $E_{\pm}^{\pi}(k_1)$, on the other hand, touch in both momenta Λ_3 and Λ_4 . This different pattern of the dispersion along the two high-symmetry lines results in the negative topological index $W_{\mathbb{Z}_2} = -1$, as formalized by Eq. (23).

B. Numerical simulations

We simulate the time evolution of an initially localized wave packet in $(1+1_{syn})$ dimensions for three different Floquet operators (all involving maximal disorder

in the real coordinate, viz. random Haar unitaries): The first simulates the topological Floquet metal, described in Eq. (20). Sharing the low energy physics of $2d$ class AII topological metallic surface states, we expect anomalous super-diffusion, $\langle \Delta X^2 \rangle \sim t \ln t$ [27], which is confirmed in Fig. 5 left panel. Numerical calculations are performed for the incommensurate frequency $\omega_2 = \sqrt{5}C$ (where the value C is indicated in the legend), and each data point is obtained from averaging over 50 disorder realizations. The second Floquet operator simulates a critical state in class A. That is, replacing the non analytic function in Eq. (20) by an analytic function, $|\sin \varphi_{2,t}| \rightarrow \sin \varphi_{2,t}$, we obtain a $(1+1_{syn})$ dimensional class A model fine-tuned to a quantum critical point separating two topologically distinct Anderson insulating phases [28]. The presence of a topological θ -term fine-tuned to the angle $\theta = \pi$ in this case protects against Anderson localization. Fig. 5 middle panel indeed indicates sub-diffusion on all accessible time scales in our numerics. Notice that the energy dispersions for the first and second Floquet operator are identical, and differences in the dynamics therefore root in the different topological terms. For the third Floquet operator, we tune the second Floquet operator away from the quantum critical point. The low energy physics in this case has a θ -term, however, with topological angle θ detuned from the critical value (see also next section). At long distances/times we then expect conventional Anderson insulating behavior, which is confirmed in the right panel of Fig. 5.

C. Incommensurability and synthetic dimensions

So far we have discussed idealized quantum walk protocols with irrational driving frequencies and frequency ratios. However, in view of our proposed experimental implementations a comment on rational approximations

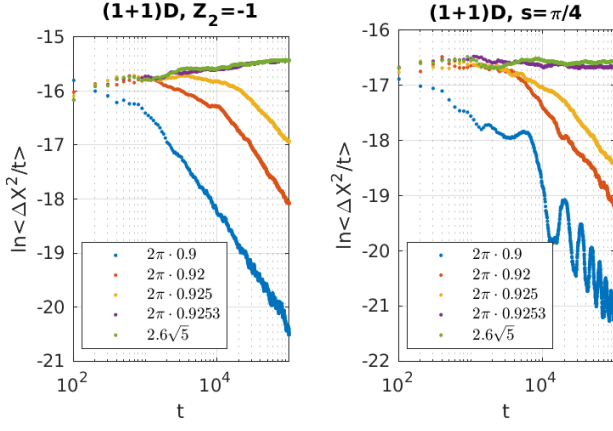


FIG. 6. Wave packet spread for quantum simulators of *finite size* class AII topological metals $\text{FM}_{1+1_{\text{syn}}}$ (left), and $2d$ class A critical metals (right). The size of the compact dimension increases with the number of decimals kept in the rational approximation α , and the dimensional crossover in the dynamics is observed at increasingly later times, see also discussion in main text.

is due. A driving frequency $\omega = 2\pi \frac{p}{q}$ generates a synthetic dimension of finite extension $\sim q$. If the dynamics on length scales $\lesssim q$ is diffusive, a dimensional crossover takes place on time scales comparable to the diffusion time associated to distance scales $\sim q$. On larger scales, the system behaves as if it lived in one dimension lower. The precision by which frequencies have to be chosen thus depends on the experimentally probed time scales: the above crossover should remain invisible in that it occurs on scales larger than the above crossover scales. (The precise value of these scales depends on system specific parameters, notably the effective diffusion constant.)

To make these general considerations more quantitative we numerically studied the protocol for the $\text{FM}_{1+1_{\text{syn}}}$ of the previous section, substituting $\omega_2 = 2.6\sqrt{5}$ by $\omega_2 = 2\pi\alpha$ with rational approximations of increasing periodicity $\alpha = 0.9, 0.92, 0.925, 0.9253$. Left Fig. 6 shows the width of a wave packet normalized by the width expected for diffusive dynamics, $\Delta X^2/t$, as a function of t on a log-log-scale. At the crossover scale to one-dimensional dynamics the (approximately) constant profile for diffusive dynamics turns into a linear slope, characteristic for localized wave packets. As anticipated, the characteristic time scale increases with the periodicity of the rational approximation, i.e. the number of decimals kept in α . Right Fig. 6 shows the corresponding numerical results for the $2d$ critical class-A metal, also discussed in the previous section.

V. LOW ENERGY PHYSICS

A. Class A

To support our claim that the protocol Eq. (10) simulates the isolated surface of a topological $4d$ quantum Hall insulator, we next apply field theory methods for disordered systems. Our aim in this section is to show that the low energy physics of both systems is described by the same effective field theory. Readers interested in more background material on field theories of disordered systems are invited to look into the supplemental material before or while plunging into this section.

To begin with, let us recall that the dispersion of the low energy excitations simulated by the clean contribution to the Floquet operator (10) is linear in k_1 and flat in all other directions. The emergence of Weyl fermions at low energies then results from the interplay of a non trivial topology and non-integrable chaotic fluctuations induced by the protocol. Indeed, we will see that the presence and stability of the Weyl fermions is topologically protected by the winding number, precisely in the same manner as the four Weyl cones of surface states in a $4d$ class A insulator at the $\nu = 4$ integer quantum Hall plateau.

Applying methods for disordered systems [29–34], we can evaluate correlation functions for the dynamical quantum walk defined by (10) in the effective quantum field theory (QFT) framework. Its matrix degree of freedom T acts in a replica space supplemented by additional causal (“retarded” and “advanced”) structure. Within such QFT the physics at long time and length scales is described by an effective action $S[T] = S_\sigma[T] + S_{\text{top}}[T]$, consisting of two contributions

$$S_\sigma = \frac{1}{8} \sum_{i,j=1}^3 \sigma_{ij}^{(0)} \text{Tr}(\partial_i Q \partial_j Q), \quad (24)$$

$$S_{\text{top}} = iW \times S_{\text{CS}}[T]. \quad (25)$$

Here the winding number W is defined in Eq. (13), with U the translational invariant part of the Floquet operator. The matrix field $Q = TQ_0T^{-1}$, is expressed as rotations around $Q_0 \equiv \sigma_3 \otimes \mathbb{1}_R$ with Pauli matrix σ_3 operating in the causal sector of the $2R$ -dimensional vector space, and ‘ $\text{Tr} = \int d^3x \text{tr}$ ’ involves the trace over the latter and $3d$ space of physical and synthetic dimensions. Readers interested in further details are invited to look into the supplemental material where we explain the mathematical structures and outline a derivation of the above action. We here restrict ourselves to a discussion of the physical implications of Eqs. (24), (25).

The first observation is that S_σ is the standard model for Anderson localization in disordered single particle systems, here in $3d$. For sufficiently strong disorder, viz. sufficiently small “bare” values $\sigma_{ij}^{(0)}$, the model flows to an Anderson insulating fixed point at long length scales with vanishing coupling constant. We here consider Haar

random disorder, for which

$$\sigma_{ij}^{(0)} = \frac{1}{2} \int d^3 \mathbf{k} \operatorname{tr}(\partial_{k_i} U_{\mathbf{k}} \partial_{k_j} U_{\mathbf{k}}^{-1}) \quad (26)$$

is purely determined by the translational invariant part of the Floquet operator. As we detailed above, we can then drive a metal-to-insulator transition by tuning the bandwidth of the system, see discussion around Eq. (14).

A game changer to the Anderson insulating scenario at strong disorder is provided by the second, topological term with Chern-Simons action S_{CS}

$$S_{\text{CS}} = \frac{1}{8\pi} \sum_{s=\pm} s \operatorname{Tr} \left(A_s \wedge dA_s + \frac{2}{3} A_s \wedge A_s \wedge A_s \right). \quad (27)$$

Here $A_s = T^{-1} dTP^s$, where $P^s = \frac{1}{2}(1 + s\sigma_3) \otimes \mathbb{1}_R$ are projectors onto the retarded ($s = +$) and advanced ($s = -$) sector of the $2R$ -dimensional vector space. The key observation then is that the combined action defined by Eqs. (24) and (25) realizes a $3d$ topological metal, which unlike systems with $W = 0$ has a conductance growing in system size even at strong disorder. In the field theory language this means that the “bare” coupling $\sigma_{ij}^{(0)}$ grows under renormalization and correlation functions show similar behavior. The same action, $S[T] = S_\sigma[T] + S_{\text{top}}[T]$, has previously been identified as describing (at length scales exceeding the mean free path) W disordered Weyl cones realized on the surface of a $4d$ class A quantum Hall insulator surface [35, 36]. We have thus established the equivalence between the protocol Eqs. (10) for driven synthetic matter and quantum Hall insulator surface states, demonstrating that both belong to the same universality class.

B. class AII

The non trivial \mathbb{Z}_2 index Eq. (22) indicates that the low energy physics of the dynamical protocol Eq. (20) is dominated by a single Weyl fermion, similar to the isolated surface of a $3d$ quantum Spin Hall insulator. The single Weyl cone is not immediate from the low energy dispersion of the clean Floquet operator Eq. (20), but rather emerges as a consequence of the non trivial topology in combination with the chaotic fluctuations induced by the protocol.

Applying field theory methods of disordered systems, we can again derive a low energy effective theory $S[T] = S_\sigma[T] + S_{\text{top}}[T]$, that allows for the calculation of correlation functions at long time and length scales. Here S_σ is the σ model action, already introduced in Eq. (24), now for the $2d$ system in the symplectic class AII. The latter alone predicts a metal-to-insulator transition for strong disorder, a scenario changed by the second, topological contribution

$$S_{\text{top}} = i \frac{\theta}{\pi} \times \Gamma[g]|_{g(0, \mathbf{x})=Q(\mathbf{x})}. \quad (28)$$

Here $\theta = \pi W_{\mathbb{Z}_2}[U]$ is the topological angle from (22), and

$$\Gamma[Q] = \frac{1}{24\pi} \int_{\mathcal{M}} \operatorname{tr}(\Phi_g \wedge \Phi_g \wedge \Phi_g) \quad (29)$$

is “half” of a Wess-Zumino-Witten action, involving the usual deformation of the field degree of freedom T . Specifically, $\Phi_g \equiv g^{-1} dg$ with $g(x_0 = 0, \mathbf{x}) = Q(\mathbf{x})$, and integration is over half the 3-torus $\mathcal{M} = [0, 1] \times [-1, 1]^2$. This topological action was previously identified [37, 38] for the description of the $3d$ disordered quantum Hall insulator. We refer the interested reader to the accompanying supplemental material for further explanations, and here only focus on a discussion of the physical implications. These are similar to those of the Chern Simons action encountered in the unitary class. For $\theta = \pi$ the system flows to a conformally invariant quantum critical point, where the coupling constant of S_σ assumes a disorder independent value (26), implying the absence of Anderson localization also for strong disorder. The same principle of delocalization is at work on $2d$ surfaces of $3d$ topological spin quantum Hall insulators. The latter are indeed described by the same effective action [37, 39], and we have thus shown that the protocol Eq. (20) belongs to the same universality class as the isolated surface of a quantum spin Hall insulator.

C. More on topological terms

The possibility for disordered systems to escape the fate of Anderson localization is signaled by topological terms in their low energy field theory description. Whether the latter are allowed depends on the dimension of the system and the target space of the field degree of freedom. The effective action of the aforementioned $3d$ class A system contains a Chern-Simons action, with coupling constant that is the winding number of the Floquet operator. The winding number and Chern Simons action signal the presence of topologically inequivalent classes of mappings

$$U_{\mathbf{k}} : \mathbb{T}^3 \mapsto \text{SU}(2), \quad (30)$$

$$Q(x_0, \mathbf{x}) : \mathbb{T}^{(3+1)} \mapsto \text{U}(2R)/[\text{U}(R) \times \text{U}(R)]. \quad (31)$$

Here the boundary configuration $Q(x_0 = 0, \mathbf{x})$ is parametrized by the $3d$ field $T(\mathbf{x})$, used in the Chern-Simons action in Eq.(27). Introducing the deformation parameter $0 \leq x_0 \leq 1$, continuously transforming the boundary value $Q(x_0 = 0, \mathbf{x})$ to the constant matrix $Q(x_0 = 1, \mathbf{x}) = \sigma_3 \otimes \mathbb{1}_R$, the Chern-Simons action can be expressed as a Wess-Zumino-Witten (WZW) term. The latter is precisely what is necessary for a $3d$ class A system to avoid Anderson localization (see supplemental material). The winding number of $U_{\mathbf{k}}$ given in (13), on the other hand, defines the coupling constant of the WZW term. That is, the combination of non-trivial homotopy groups $\pi_3(\text{SU}(2)) = \mathbb{Z}$ and $\pi_4(\text{U}(2R)/[\text{U}(R) \times \text{U}(R)]) = \mathbb{Z}$ allows for non-vanishing coupling constants

weighting topologically non-trivial field configurations $T(\mathbf{x})$.

For the $2d$ quantum spin Hall surface states it is the emergence of a WZW action, weighted by a \mathbb{Z}_2 topological angle in the effective low energy description that allows for topological metallic phases. The involved maps in momentum- and real-space read

$$U_{\mathbf{k}} : \mathbb{T}^2 \mapsto \text{U}(2)/\text{Sp}(2), \quad (32)$$

$$Q(\mathbf{x}) : \mathbb{T}^2 \mapsto \text{O}(4R)/[\text{O}(2R) \times \text{O}(2R)], \quad (33)$$

with non trivial homotopy groups, $\pi_2(\text{U}(2)/\text{Sp}(2)) = \mathbb{Z}_2$ and $\pi_2(\text{O}(4R)/[\text{O}(2R) \times \text{O}(2R)]) = \mathbb{Z}_2$, respectively. Both maps are thus characterized by non trivial \mathbb{Z}_2 indices, and we already introduced a topological \mathbb{Z}_2 invariant for the Floquet operator Eq. (32) in Eq. (22). Alternatively, one can express the \mathbb{Z}_2 index as “half” of a Wess-Zumino-Witten term, which is readily extended to Eq. (33), see also supplemental material for more details.

We conclude remarking that the above discussion only relies on general structures, such as the softmode manifold identified in the course of the construction of the effective field theory, and applies as a matter of principle. Whether there exist physical systems characterized by non-trivial couplings is an independent issue. The models we propose in the earlier sections are one option how to realize non trivial mappings utilizing the idea of engineered synthetic dimension. That is, in the present work we provide the field theories, physical models, and numerical confirmation of topological Floquet metals for both complex and real symmetry classes, which are characterized by \mathbb{Z} and \mathbb{Z}_2 topological indices, respectively. The presented structures encompass topological Floquet metal in other dimension and symmetry classes.

VI. DISCUSSION

In this paper, we have introduced quantum simulators for topological surface states in isolation. Our proposal sidesteps the bulk boundary principle and overcomes the fermion doubling theorem, impeding the realization of isolated surface states in generic solid state (lattice) systems. The key element of our proposal is the dynamical generation of physical dimensions via external driving, using incommensurate frequencies. The simulation of extra dimensions via driving physical platforms has already been used in cold atom systems to measure the Anderson localization-delocalization transition in three dimensions to a degree of resolution not reachable in solid state materials. We here apply the idea to one-dimensional quantum walks of a spin-1/2 particle with time dependent spin rotation matrices, viz. “coin operations”, following multi-frequency dynamical protocols. The latter provide a flexibility absent in lattice systems, which allows for the simulation of (gauge) equivalent real-space dynamics involving long range hopping.

We have illustrated the general idea on two specific examples, the three-dimensional topological surface states

of a four-dimensional quantum Hall insulator, and the two-dimensional surface states of a three-dimensional spin quantum Hall insulator. An inherent feature of both protocols is that the artificial generation of “synthetic” dimensions induces diffusive dynamics in all (gauge) equivalent space directions after already a few iterations of the protocol, as verified in numerical simulations. Our approach, thus, simulates the surfaces of “disordered” phases lacking translational invariance, which adds an element of realism. For both examples, we identified topological invariants showing the non trivial topological nature of the dynamical protocols. Comparing simulations of the latter to that of topologically trivial parents with variable disorder strengths (respectively bandwidth) clearly shows the impact of a non trivial topology. While strong disorder turns the simulators of trivial metals into Anderson insulators, no signature of localization is found for the topological non trivial protocols for all disorder strengths, respectively, bandwidths. Importantly, the numerical simulations show differences in the dynamics simulated by the different protocols already after an experimentally accessible number of $\sim \mathcal{O}(20)$ time steps. This also sets the precision to which frequencies have to be chosen in experiment. Approximating irrational numbers by rational generates *finite* rather than infinitely extended synthetic dimensions. As long as the corresponding diffusion time (i.e. the time required to explore the finite dimension) exceeds the time scales probed in experiment, protocols with rational numbers can be used for all practical purposes.

Employing field theory methods, we have shown that the quantum simulators generate dynamics within the same universality class as the corresponding topological insulator surface states. Specifically, we demonstrated that the universal long-time dynamics of the dynamical protocol is described by precisely the same topological field theory also proposed for the simulated surface states. The field theory construction builds on the color-flavor transformation, and can be readily generalized to other symmetry classes and dimensions. Generalizing e.g. the simulator of topological quantum Hall surface states to other (odd) dimensions, different from three, one can derive the corresponding Chern Simons actions. Similarly, a topological field theory with Chern Simons action can be derived for the simulator probing the surface states of a quantum spin Hall insulator (‘class AII’) in four dimensions, and different from the \mathbb{Z}_2 field theory in three dimensions discussed here in detail. An exception is provided by class AIII systems. These cannot be simulated within the proposed scheme, since the gauge transformation, establishing the equivalence between the periodically driven and higher dimensional system, breaks chiral symmetry.

Our proposal requires full dynamical control over a two-state internal degree of freedom (“spin”), which at the current state may be difficult to achieve in optical lattices. We, therefore, focused on the alternative platform of linear optical networks, similar to that used in Ref. [8].

Specifically, time-multiplexing networks with fast switching electro-optic modulators seem promising candidates for the implementation of the quantum simulators. We provided detailed blueprints for the experimental implementation of the two protocols within existing set ups, realizing the quantum simulators of the surface states of a four dimensional quantum Hall insulator and a three dimensional quantum spin Hall insulator. We have shown in our numerical simulations that the experimental signature, viz. absence of Anderson localization, is observable within the experimentally realizable number of time steps. A tunable quantum simulator of topological surface states in isolation, would open fascinating experimental possibilities. Specifically, it would provide a new, direct window into the intriguing physics resulting from the interplay of disorder and non trivial topology.

Acknowledgments:—T. M. acknowledges financial support by Brazilian agencies CNPq and FAPERJ. K.W.K. acknowledges financial support by Basic Science Research Program through the National Research Foundation of Korea (NRF) funded by the Ministry of Education (20211060) and Korea government(MSIT) (No.2020R1A5A1016518). A.A. and D.B. were funded by the Deutsche Forschungsgemeinschaft (DFG) Projektnummer 277101999 TRR 183 (project A01/A03).

Appendix A: Unitarity of quantum walk operator

The general single time-step operator Eq. (1) simplifies to Eq. (2) when focusing on quantum walks with short range hopping $m = \{-1, 0, +1\}$. In momentum-representation,

$$\hat{U}_{\mathbf{k}} = \sum_{m=0,\pm} (\vec{r}_m \cdot \vec{\sigma}) e^{imk_1}, \quad (\text{A1})$$

$$= [\vec{r}_0 + (\vec{r}_+ + \vec{r}_-) \cos k_1 + i(\vec{r}_+ - \vec{r}_-) \sin k_1] \cdot \vec{\sigma},$$

where \vec{r}_m is a four-component vector and $\vec{\sigma} = (\sigma_0, i\vec{\sigma})$. To satisfy unitarity, the vector multiplying $\vec{\sigma}$ must be real valued, that is, $\vec{r}_+ = (\vec{r}_-)^*$. Expressing $\vec{r}_+ = (\vec{r}_r + i\vec{r}_i)$ in terms of two real vectors \vec{r}_r, \vec{r}_i ,

$$\hat{U}_{\mathbf{k}} = [\vec{r}_0 + (\vec{r}_r + i\vec{r}_i)e^{ik_1} + (\vec{r}_r - i\vec{r}_i)e^{-ik_1}] \cdot \vec{\sigma}, \quad (\text{A2})$$

and requiring further that $\hat{U}_{\mathbf{k}}\hat{U}_{\mathbf{k}}^\dagger = \mathbb{1}$, the following relations can be verified

$$\begin{aligned} |\vec{r}_0|^2 + |\vec{r}_-|^2 + |\vec{r}_+|^2 &= 1, \\ |\vec{r}_0|^2 + 2|\vec{r}_r|^2 + 2|\vec{r}_i|^2 &= 1, \\ \vec{r}_r \cdot \vec{r}_i &= 0, \vec{r}_r \cdot \vec{r}_0 = 0, \vec{r}_i \cdot \vec{r}_0 = 0, \\ |\vec{r}_r| &= |\vec{r}_i| = \frac{1}{2}\sqrt{1 - |\vec{r}_0|^2}. \end{aligned} \quad (\text{A3})$$

These are stated below Eq. (2) in the main text.

Appendix B: Spreading of a wave packet

In this Appendix we demonstrate the equivalence of Eqs. (7 and (8). To this end we introduce the initial density matrix

$$\rho_0 = \frac{1}{N_{\text{syn}}} \sum_{k_{\text{syn}}, \sigma} |0, k_{\text{syn}}, \sigma\rangle \langle 0, k_{\text{syn}}, \sigma|, \quad \rho_0^2 = \rho_0, \quad (\text{B1})$$

(here $n_1 = 0$ refers to the origin in the physical space and $N_{\text{syn}} \gg 1$ is the number of initial phases) and note that Eqs. (7) for ΔX^2 can be cast in the basis independent form

$$\langle \Delta X^2 \rangle = \text{tr} \left(\overline{\hat{\rho}_0 \mathcal{U}_{t,0}^\dagger \hat{n}_1^2 \mathcal{U}_{t,0}} \right), \quad (\text{B2})$$

where $\overline{(\dots)}$ refers to a disorder average. The rationale behind this expression is the following. The average over initial phases (momenta k_{syn}) implies the trace operation in the extended Hilbert space, and we discretize the corresponding momentum integral so that it becomes a sum over N_{syn} terms.

Applying further the time-dependent gauge transformation introduced in section II A one writes

$$\mathcal{U}_{t,0} = e^{it \sum_{j \geq 2} \omega_j \hat{n}_j} \mathcal{U}_F^t, \quad (\text{B3})$$

where the Floquet operator \mathcal{U}_F was defined in Eq. (6). This ansatz gives us the equivalent expression for the width of a wave packet,

$$\langle \Delta X^2 \rangle = \text{tr} \left(\hat{\rho}_0 (\mathcal{U}_F^\dagger)^t \hat{n}_1^2 \mathcal{U}_F^t \right). \quad (\text{B4})$$

Lastly, to evaluate the trace above one can use a full coordinate representation, which gives us

$$\langle \Delta X^2 \rangle = \frac{1}{N_{\text{syn}}} \sum_{\mathbf{n}, \mathbf{n}', \sigma, \sigma'} n_1^2 |\langle \mathbf{n}', \sigma' | \mathcal{U}_F^t | \mathbf{n}, \sigma \rangle|^2, \quad (\text{B5})$$

with $|\mathbf{n}, \sigma\rangle \equiv |n_1, n_{\text{syn}}, \sigma\rangle$ and $|\mathbf{n}', \sigma'\rangle \equiv |n_1, n'_{\text{syn}}, \sigma'\rangle$. We then notice that upon a disorder average the transition probability depends only on the difference in position, $\mathbf{n}' - \mathbf{n}$, and thereby the expression (8) in the main text is recovered.

Appendix C: Blueprint for the FM_{1+1syn} simulator

A detailed blueprint for the optical linear network simulating the topological FM_{1+1syn} is shown in Fig. 7. The dynamical protocol, Eq. (20), involving all three components $\hat{R}_{\pm,0}$ requires a more complex set-up in comparison to FM_{1+2syn} in class A, which now has to be build from two chiral half-step and two coin operations. Therefore we start by summarizing the optical scheme in Fig. 7 and then provide its justification. To this end we decompose

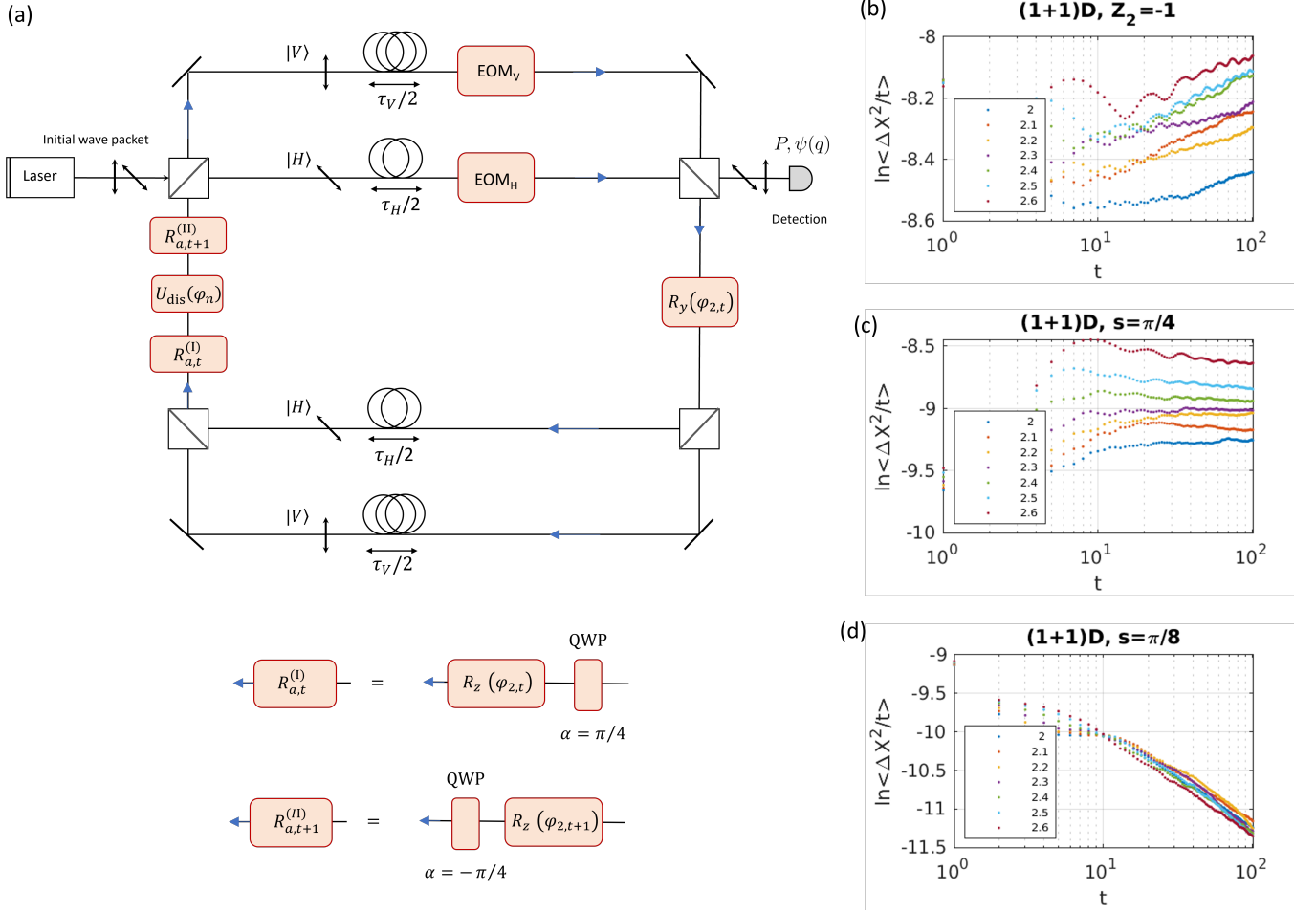


FIG. 7. Blueprint of an optical linear network simulating the topological surface states of a $3d$ quantum spin Hall insulator in the quantum walk setting. (a) The feedback loop is build of the step operator $\hat{T}_C^{\pm \frac{1}{2}}$ (upper and middle arms, respectively) and the coin operators \hat{R}_a and \hat{R}_b (right and left arm, respectively), for details see main text. To the left and right of the loop, source and detection units are connected. (b) Numerical simulation of a topological metal ($\mathbb{Z}_2 = -1$) in a $(1 + 1_{\text{syn}})D$ quantum walk for short time steps accessible by experiments. The width of the wave packet scaled by time is plotted on a log-scale, showing that diffusion is anomalously fast. (c) Critical quantum walk in $(1 + 1_{\text{syn}})D$ class A at a topological quantum phase transition, showing the same scaling with the classical diffusion $\langle \Delta X^2 \rangle \sim t$. (d) Quantum walk in $(1 + 1_{\text{syn}})D$ class A without topological term, showing Anderson localization. Colors correspond to incommensurate frequencies $\omega_2 = \sqrt{5}C$ with values for C as indicated in the legends.

the translational invariant part of the single time step evolution operator, Eq. (20), into the product

$$\mathcal{U}_{t+1,t} = \hat{U}_{\text{dis}} \hat{R}_a(t) \hat{T}_C^{\frac{1}{2}} \hat{R}_b(t) \hat{T}_C^{\frac{1}{2}}, \quad (\text{C1})$$

of a chiral half-step, $\hat{T}_C^{\frac{1}{2}}$, and coin operators, $\hat{R}_{a/b}$. (The former are positioned in the four horizontal arms, notice the half fiber lengths $\tau_H/2$ and $\tau_V/2$, and the latter are placed in the vertical arms.) Dynamical EOMs after fiber lines of the first step operation allow to terminate the walk by sending the photons to the detection unit. The coin operators are chosen as

$$\hat{R}_b(t) = Y R_z(-\varphi_{2,t}) Y^\dagger \equiv R_y(\varphi_{2,t}), \quad (\text{C2})$$

where $Y = e^{i\pi\sigma_1/4}$ is the matrix of y -basis change [25], and $\hat{R}_a(t) = \hat{R}_{a,t+1}^{(\text{II})} \hat{R}_{a,t}^{(\text{I})}$, with

$$\hat{R}_{a,t}^{(\text{I})} = \begin{cases} R_z(\varphi_{2,t}) \hat{Y}^\dagger, & \sin \varphi_{2,t} \geq 0, \\ \hat{Y}^\dagger, & \sin \varphi_{2,t} < 0, \end{cases} \quad (\text{C3})$$

and

$$\hat{R}_{a,t+1}^{(\text{II})} = \begin{cases} \hat{Y}, & \sin \varphi_{2,t+1} \geq 0, \\ \hat{Y} R_z(\varphi_{2,t+1}), & \sin \varphi_{2,t+1} < 0, \end{cases} \quad (\text{C4})$$

with $\varphi_{2,t} = k_2 + \omega_2 t$. Finally, disorder is introduced by placing in between $\hat{R}_{a,t}^{(\text{I})}$ and $\hat{R}_{a,t+1}^{(\text{II})}$ the local, time reversal invariant random potential $U(n_1) = e^{i\phi_{n_1}\sigma_0}$, with

position dependent angles ϕ_{n_1} , randomly drawn from the unit circle $-\pi \leq \phi_{n_1} < \pi$.

Coming back to the justification of (C1) we note that expressing the time evolution operator in Eq. (20) as the product of elementary chiral translations and coin operators is not immediately straightforward. To start with, we first notice that upon replacing $|\sin k_2| \rightarrow \sin k_2$ in Eq.(21), the model is reduced to the familiar 2d class A Floquet insulator [28, 40], which is built by the multiplication of simpler operators. For an implementation of the protocol with absolute value $|\sin k_2|$, we separate cases $\sin k_2 \leq 0$ and $\sin k_2 > 0$. Specifically, a class A 2d Floquet model with homotopy parameter s is written as [28] the product of four unitary operators $\hat{U}_A = \hat{U}_4 \hat{U}_3 \hat{U}_2 \hat{U}_1$, with

$$\hat{U}_i(k) = \cos(s) + i \sin(s) \begin{pmatrix} & e^{-i\mathbf{k} \cdot \mathbf{v}_i} \\ e^{i\mathbf{k} \cdot \mathbf{v}_i} & \end{pmatrix}.$$

Here $(\mathbf{v}_1, \mathbf{v}_2, \mathbf{v}_3, \mathbf{v}_4) = (0, -\mathbf{e}_1, -\mathbf{e}_1 + \mathbf{e}_2, \mathbf{e}_2)$, with $\mathbf{e}_{1,2}$ lattice unit vectors in the horizontal/vertical direction. At $s = \pi/4$, the product of unitaries can be expanded in the quantum walk form

$$\hat{U}_A = (\hat{r}_0 \cdot \vec{\sigma}) + (\vec{r}_+ \cdot \vec{\sigma})e^{ik_1} + (\vec{r}_- \cdot \vec{\sigma})e^{-ik_1},$$

where

$$\begin{aligned} \vec{r}_0 &= \frac{1}{2}(1 - \cos k_2, 0, 0, \sin k_2), \\ \vec{r}_+ &= \frac{1}{4}(-1 - \cos k_2, 0, 0, \sin k_2), \\ \vec{r}_- &= \frac{1}{4}(0, \sin k_2, -1 - \cos k_2, 0). \end{aligned}$$

Following the general recipe outlined in Sec. II A, we simulate the 2d dynamics as a 1d quantum walk with time dependent protocol, replacing momentum $k_2 \rightarrow \varphi_{2,t}$ by a time dependent angle. We then notice that for $\sin \varphi_{2,t} > 0$ vectors $\vec{r}_{0,r,i}$ of \hat{U}_A are identical to that of \hat{U}_{AII} in Eq.(20). Hence, when $\sin \varphi_{2,t} > 0$, the quantum walk operator in Eq.(20) can be written as the product of the four unitary operators, $\hat{U}_{\text{AII}}(\sin \varphi_{2,t} > 0) = \hat{U}_A(k_1, \varphi_{2,t})$. When $\sin \varphi_{2,t} < 0$, on the other hand, one can verify that $\hat{U}_{\text{AII}, \sin \varphi_{2,t} < 0}(k_1, \varphi_{2,t}) = \hat{U}_A^T(-k_1, \varphi_{2,t}, s = \frac{\pi}{4})$.

Next, we express $\hat{U}_{j=1,2,3,4}$ as a combination of shift and rotation operators,

$$\begin{aligned} \hat{U}_1 &= e^{is\sigma_1}, \\ \hat{U}_2 &= \hat{T}_C^{-\frac{1}{2}} e^{is\sigma_1} \hat{T}_C^{\frac{1}{2}}, \\ \hat{U}_3 &= e^{i\varphi_{2,t}\sigma_3/2} \hat{T}_C^{-\frac{1}{2}} e^{is\sigma_1} \hat{T}_C^{\frac{1}{2}} e^{-i\varphi_{2,t}\sigma_3/2}, \\ \hat{U}_4 &= e^{i\varphi_{2,t}\sigma_3/2} e^{is\sigma_1} e^{-i\varphi_{2,t}\sigma_3/2}, \end{aligned}$$

with ‘half’ translation operator $\hat{T}_C^{\frac{1}{2}} = e^{ik_1\sigma_3/2}$. We stress that the full Floquet operator \hat{U}_A is 2π periodic in k_1 and the appearance of a ‘half’ translation operator does not imply a doubling of the unit cell. The same is true for the topological Floquet metal model.

The 2d class AII model is expressed as

$$\begin{aligned} \hat{U}_{\text{AII}, \sin \varphi_{2,t} \geq 0}(k_1, \varphi_{2,t}) & \\ &= \hat{U}_A(k_1, \varphi_{2,t}, s = \frac{\pi}{4}) \\ &= e^{i\varphi_{2,t}\sigma_3/2} Y \hat{T}_C^{-\frac{1}{2}} Y e^{-i\varphi_{2,t}\sigma_3/2} Y \hat{T}_C^{\frac{1}{2}} Y, \\ &= -e^{i\varphi_{2,t}\sigma_3/2} Y^\dagger \hat{T}_C^{\frac{1}{2}} Y^\dagger e^{-i\varphi_{2,t}\sigma_3/2} Y \hat{T}_C^{\frac{1}{2}} Y, \end{aligned} \quad (\text{C5})$$

and to arrive at this result we used that $Y \hat{T}_C^{-\frac{1}{2}} Y = -Y^\dagger \hat{T}_C^{\frac{1}{2}} Y^\dagger$ and commutativity of operators $\hat{T}_C^{\frac{1}{2}}$ and $e^{-i\varphi_{2,t}\sigma_3/2}$. On the other hand,

$$\begin{aligned} \hat{U}_{\text{AII}, \sin \varphi_{2,t} < 0}(k_1, \varphi_{2,t}) & \\ &= \hat{U}_A^T(-k_1, \varphi_{2,t}, s = \frac{\pi}{4}) \\ &= Y \hat{T}_C^{-\frac{1}{2}} Y e^{-i\varphi_{2,t}\sigma_3/2} Y \hat{T}_C^{\frac{1}{2}} Y e^{i\varphi_{2,t}\sigma_3/2}, \\ &= -Y^\dagger \hat{T}_C^{\frac{1}{2}} Y^\dagger e^{-i\varphi_{2,t}\sigma_3/2} Y \hat{T}_C^{\frac{1}{2}} Y e^{i\varphi_{2,t}\sigma_3/2}, \end{aligned} \quad (\text{C6})$$

and from above relations (C5) and (C6) we notice that $\hat{U}_{\text{AII}} = R_a^{(\text{I})} \hat{T}_C^{\frac{1}{2}} R_b \hat{T}_C^{\frac{1}{2}} R_a^{(\text{II})}$. Up to a cyclic permutation of the operator $R_a^{(\text{II})}$ this is equivalent to the clean part of $\mathcal{U}_{t+1,t}$, see Eq. (C1). Notice that in both cases \hat{U}_{AII} involves the same unitary sandwiched between the two $\hat{T}_C^{\frac{1}{2}}$, which simplifies the implementation of $\hat{R}_b(t) = Y^\dagger e^{-i\varphi_{2,t}\sigma_3/2} Y$. $\hat{R}_a(t)$, on the other hand, depends on the sign of $\sin \varphi_{2,t}$.

Appendix D: \mathbb{Z}_2 topological invariant

In this Appendix we further discuss the \mathbb{Z}_2 topological invariant for the 2-band model and prove the relation (23). The unitary operator $\hat{U}_{\mathbf{k}}$ gives rise to the auxiliary Hamiltonian [3, 41],

$$\tilde{H}_U(\mathbf{k}) = \begin{pmatrix} 0 & U_{\mathbf{k}} \\ U_{\mathbf{k}}^\dagger & 0 \end{pmatrix}, \quad (\text{D1})$$

which shares time-reversal and particle-hole symmetries, $\hat{\Theta}_1 \tilde{H}_U(\mathbf{k}) \hat{\Theta}_1^{-1} = \tilde{H}_U(-\mathbf{k})$, and $\hat{\Theta}_2 \tilde{H}_U(\mathbf{k}) \hat{\Theta}_2^{-1} = -\tilde{H}_U(-\mathbf{k})$, respectively, with $\hat{\Theta}_1 = \tau_1 \otimes i\sigma_2 \mathcal{K}$, and $\hat{\Theta}_2 = i\tau_2 \otimes i\sigma_2 \mathcal{K}$. That is, H_U belongs to class DIII. Notice that in Eq.(D1) off diagonal elements are the Floquet unitary operator without band flattening. This allows us to make a connection between the \mathbb{Z}_2 invariant and the eigen-energies at time-reversal invariant momenta.

A way to compute the \mathbb{Z}_2 topological invariant then is as follows [26]: The Hamiltonian has two valence bands at energy $E = -1$, and their eigenvectors are

$$u_1^-(\mathbf{k}) = \frac{1}{\sqrt{2}} \begin{pmatrix} -1 \\ 0 \\ U_{\mathbf{k},11}^* \\ U_{\mathbf{k},12}^* \end{pmatrix}, \quad u_2^-(\mathbf{k}) = \frac{1}{\sqrt{2}} \begin{pmatrix} 0 \\ -1 \\ U_{\mathbf{k},21}^* \\ U_{\mathbf{k},22}^* \end{pmatrix}, \quad (\text{D2})$$

where $U_{\mathbf{k},ij}^* = (U_{\mathbf{k}}^\dagger)_{ji}$. The sewing matrix, needed to compute the topological invariant [26], can be obtained from these two vectors as $(w_{\mathbf{k}})_{ab} = \langle u_a^-(-\mathbf{k}) | \hat{\Theta}_1 u_b^-(\mathbf{k}) \rangle$. That is,

$$w_{\mathbf{k}} = \frac{1}{2} \begin{pmatrix} -U_{\mathbf{k},12} + U_{-\mathbf{k},12} & -U_{\mathbf{k},22} - U_{-\mathbf{k},11} \\ U_{\mathbf{k},11} + U_{-\mathbf{k},22} & U_{\mathbf{k},21} - U_{-\mathbf{k},21} \end{pmatrix}, \quad (\text{D3})$$

$$= \begin{pmatrix} -U_{\mathbf{k},12} & -U_{\mathbf{k},22} \\ U_{\mathbf{k},11} & U_{\mathbf{k},21} \end{pmatrix}, \quad (\text{D4})$$

$$= -i\sigma_2 U_{\mathbf{k}}^T, \quad (\text{D5})$$

where in the second line time-reversal symmetry of the unitary operator was used, i.e. $U_{\mathbf{k},11} = U_{-\mathbf{k},22}$, $U_{\mathbf{k},12} = -U_{-\mathbf{k},12}$ and $U_{\mathbf{k},21} = -U_{-\mathbf{k},21}$ (as follows from $\sigma_2 U_{\mathbf{k}} \sigma_2 = U_{-\mathbf{k}}^T$). One can then readily verify that the sewing ma-

trix is anti-symmetric at time-reversal invariant momenta $\Lambda_1 = (0,0)$, $\Lambda_2 = (\pi,0)$, $\Lambda_3 = (0,\pi)$, and $\Lambda_4 = (\pi,\pi)$, i.e.

$$w_{\Lambda_j} = \frac{1}{2} \begin{pmatrix} 0 & -U_{\Lambda_j,11} - U_{\Lambda_j,22} \\ U_{\Lambda_j,11} + U_{\Lambda_j,22} & 0 \end{pmatrix}, \quad (\text{D6})$$

where $U_{\Lambda_j,11} = U_{\Lambda_j,22}$, and the Pfaffian is $\text{Pf}[w_{\Lambda_j}] = -\frac{1}{2}(U_{\Lambda_j,11} + U_{\Lambda_j,22}) = -\frac{1}{2}\text{tr}[U_{\Lambda_j}] = -\exp(i\epsilon_{\Lambda_j})$. Finally, the \mathbb{Z}_2 topological invariant becomes

$$W_{\mathbb{Z}_2} = \prod_{j=1,2,3,4} \text{Pf}[w_{\Lambda_j}] = \exp\left(i \sum_{j=1,2,3,4} \epsilon_{\Lambda_j}\right), \quad (\text{D7})$$

which implies that the condition for a non trivial Floquet topological metal, $W_{\mathbb{Z}_2} = -1$, translates into $\sum_{j=1,2,3,4} \epsilon_{\Lambda_j} = \pi \pmod{2\pi}$.

-
- [1] B. Sbierski, J. F. Karcher, and M. S. Foster, Spectrum-Wide Quantum Criticality at the Surface of Class AIII Topological Phases: An “Energy Stack” of Integer Quantum Hall Plateau Transitions, *Phys. Rev. X* **10**, 021025 (2020).
- [2] X.-Q. Sun, M. Xiao, T. c. v. Bzdušek, S.-C. Zhang, and S. Fan, Three-dimensional chiral lattice fermion in floquet systems, *Phys. Rev. Lett.* **121**, 196401 (2018).
- [3] S. Higashikawa, M. Nakagawa, and M. Ueda, Floquet chiral magnetic effect, *Phys. Rev. Lett.* **123**, 066403 (2019).
- [4] J. Chabé, G. Lemarié, B. Grémaud, D. Delande, P. Szriftgiser, and J. C. Garreau, Experimental observation of the anderson metal-insulator transition with atomic matter waves, *Phys. Rev. Lett.* **101**, 255702 (2008).
- [5] G. Lemarié, J. Chabé, P. Szriftgiser, J. C. Garreau, B. Grémaud, and D. Delande, Observation of the anderson metal-insulator transition with atomic matter waves: Theory and experiment, *Phys. Rev. A* **80**, 043626 (2009).
- [6] A. Schreiber, A. Gábris, P. P. Rohde, K. Laiho, M. Štefaniák, V. Potoček, C. Hamilton, I. Jex, and C. Silberhorn, A 2d quantum walk simulation of two-particle dynamics, *Science* **336**, 55 (2012).
- [7] L. Lorz, E. Meyer-Scott, T. Nitsche, V. Potoček, A. Gábris, S. Barkhofen, I. Jex, and C. Silberhorn, Photonic quantum walks with four-dimensional coins, *Phys. Rev. Research* **1**, 033036 (2019).
- [8] A. Gerdali, S. De, A. Laneve, S. Barkhofen, J. Sperling, P. Mataloni, and C. Silberhorn, Transient subdiffusion via disordered quantum walks, *Phys. Rev. Research* **3**, 023052 (2021).
- [9] G. Casati, I. Guarneri, and D. L. Shepelyansky, Anderson transition in a one-dimensional system with three incommensurate frequencies, *Phys. Rev. Lett.* **62**, 345 (1989).
- [10] F. Haake, *Quantum Signatures of Chaos* (Springer-Verlag, Berlin, Heidelberg, 2006).
- [11] D. L. Shepelyansky, Localization of quasienergy eigenfunctions in action space, *Phys. Rev. Lett.* **56**, 677 (1986).
- [12] F. L. Moore, J. C. Robinson, C. Bharucha, P. E. Williams, and M. G. Raizen, Observation of dynamical localization in atomic momentum transfer: A new testing ground for quantum chaos, *Phys. Rev. Lett.* **73**, 2974 (1994).
- [13] C. Tian and A. Altland, Theory of localization and resonance phenomena in the quantum kicked rotor, *New Journal of Physics* **12**, 043043 (2010).
- [14] G. Lemarié, H. Lignier, D. Delande, P. Szriftgiser, and J. C. Garreau, Critical state of the anderson transition: Between a metal and an insulator, *Phys. Rev. Lett.* **105**, 090601 (2010).
- [15] C. Tian, Y. Chen, and J. Wang, Emergence of integer quantum Hall effect from chaos, *Phys. Rev. B* **93**, 075403 (2016).
- [16] I. Martin, G. Refael, and B. Halperin, Topological frequency conversion in strongly driven quantum systems, *Phys. Rev. X* **7**, 041008 (2017).
- [17] E. J. Meier, F. A. An, A. Dauphin, M. Maffei, P. Massignan, T. L. Hughes, and B. Gadway, Observation of the topological anderson insulator in disordered atomic wires, *Science* **362**, 929 (2018).
- [18] A. Schreiber, K. N. Cassemiro, V. Potoček, A. Gábris, P. J. Mosley, E. Andersson, I. Jex, and C. Silberhorn, Photons walking the line: A quantum walk with adjustable coin operations, *Phys. Rev. Lett.* **104**, 050502 (2010).
- [19] J. P. Dahlhaus, J. M. Edge, J. Tworzydło, and C. W. J. Beenakker, Quantum Hall effect in a one-dimensional dynamical system, *Phys. Rev. B* **84**, 115133 (2011).
- [20] J. M. Edge, J. Tworzydło, and C. W. J. Beenakker, Metallic Phase of the Quantum Hall Effect in Four-Dimensional Space, *Phys. Rev. Lett.* **109**, 135701 (2012).
- [21] C. Tian, Y. Chen, and J. Wang, Emergence of integer quantum Hall effect from chaos, *Phys. Rev. B* **93**, 075403 (2016).
- [22] I. Petrides, H. M. Price, and O. Zilberberg, Six-dimensional quantum Hall effect and three-dimensional topological pumps, *Phys. Rev. B* **98**, 125431 (2018).
- [23] For $n \neq \pm 1$, $\int_{-\pi}^{\pi} e^{ik_2 n} |\sin k_2| dk_2 = \frac{2}{n^2-1}((-1)^{n+1} - 1)$.
- [24] M. S. Rudner, N. H. Lindner, E. Berg, and M. Levin, Anomalous edge states and the bulk-edge correspondence for periodically driven two-dimensional systems, *Phys.*

- Rev. X **3**, 031005 (2013).
- [25] For example, rotation around y-axis, $\hat{R}_2(\varphi) = e^{i\pi\sigma_1/4}\hat{R}_3(\varphi)e^{-i\pi\sigma_1/4}$, is implemented using the quarter-wave plates aligned at an angle $\pi/4$, $\hat{C}_{\text{QWP}}(\pi/4) = e^{-i\pi\sigma_1/4}$ [8]. While the rotation around x-axis, $\hat{R}_1(\varphi) = e^{-i\pi\sigma_2/4}\hat{R}_3(\varphi)e^{i\pi\sigma_2/4}$, is implemented by using the two half wave plates: $\hat{C}_{\text{HWP}}(\pi/8)\hat{C}_{\text{HWP}}(0) = e^{-i\pi\sigma_2/4}$ [18].
- [26] S. Ryu, A. P. Schnyder, A. Furusaki, and A. W. W. Ludwig, Topological insulators and superconductors: tenfold way and dimensional hierarchy, New Journal of Physics **12**, 065010 (2010).
- [27] C. Tian, Anomalous quantum diffusion and the topological metal, Phys. Rev. B **86**, 121304 (2012).
- [28] K. W. Kim, D. Bagrets, T. Micklitz, and A. Altland, Quantum Hall criticality in Floquet topological insulators, Phys. Rev. B **101**, 165401 (2020).
- [29] F. Wegner, The mobility edge problem: Continuous symmetry and a conjecture, Zeitschrift für Physik B: Condensed Matter **35**, 207 (1979).
- [30] K. B. Efetov, A. I. Larkin, and D. E. Khmel'nitskii, Interaction of diffusion modes in the theory of localization, JETP **52**, 568 (1980).
- [31] A. M. Pruisken and L. Schäfer, The Anderson model for electron localisation non-linear σ model, asymptotic gauge invariance, Nuclear Physics B **200**, 20 (1982).
- [32] K. B. Efetov and A. I. Larkin, Kinetics of a quantum particle in long metallic wires, Sov. Phys. JETP **58**, 444 (1983).
- [33] A. Pruisken, On localization in the theory of the quantized Hall effect: A two-dimensional realization of the θ -vacuum, Nuclear Physics B **235**, 277 (1984).
- [34] K. B. Efetov, *Synergism in Disorder and Chaos* (Cambridge University Press, Cambridge, 1997).
- [35] A. Altland and D. Bagrets, Theory of the strongly disordered Weyl semimetal, Phys. Rev. B **93**, 075113 (2016).
- [36] Y. X. Zhao and Z. D. Wang, General response theory of topologically stable Fermi points and its implications for disordered cases, Phys. Rev. B **92**, 085143 (2015).
- [37] S. Ryu, C. Mudry, H. Obuse, and A. Furusaki, \mathbb{Z}_2 topological term, the global anomaly, and the two-dimensional symplectic symmetry class of anderson localization, Phys. Rev. Lett. **99**, 116601 (2007).
- [38] E. J. König, P. M. Ostrovsky, I. V. Protopopov, I. V. Gornyi, I. S. Burmistrov, and A. D. Mirlin, Interaction and disorder effects in three-dimensional topological insulator thin films, Phys. Rev. B **88**, 035106 (2013).
- [39] P. M. Ostrovsky, I. V. Gornyi, and A. D. Mirlin, Quantum criticality and minimal conductivity in graphene with long-range disorder, Phys. Rev. Lett. **98**, 256801 (2007).
- [40] M. S. Rudner, N. H. Lindner, E. Berg, and M. Levin, Anomalous edge states and the bulk-edge correspondence for periodically driven two-dimensional systems, Phys. Rev. X **3**, 031005 (2013).
- [41] R. Roy and F. Harper, Periodic table for Floquet topological insulators, Phys. Rev. B **96**, 155118 (2017).
- [42] M. R. Zirnbauer, Riemannian symmetric superspaces and their origin in random-matrix theory, Journal of Mathematical Physics **37**, 4986 (1996).
- [43] A. Altland and M. R. Zirnbauer, Nonstandard symmetry classes in mesoscopic normal-superconducting hybrid structures, Physical Review B **55**, 1142 (1997).
- [44] M. R. Zirnbauer, Supersymmetry for systems with unitary disorder: circular ensembles, Journal of Physics A: Mathematical and General **29**, 7113 (1996).
- [45] Note that for such construction $U(\pi/2, k) \rightarrow -i\sigma_3$, which is not yet time-reversal symmetric operator. However, a subsequent rotation $e^{i\psi\sigma_3}(-i\sigma_3)$ with $\psi \in [0, \pi/2]$ brings it to the identity matrix σ_0 . At this interval a spectral density in (S28) is zero thereby giving no contribution to θ -angle.

Supplemental Materials

In this supplemental material we provide details on the effective field theory description of the quantum simulator protocols. We start out with a brief review of the standard effective field theory for disordered single particle systems, then outline how to map the protocols discussed in the main text to the latter, and finally deepen our discussion of topological terms.

S1. FIELD THEORY REVIEW

A. Diffusive non-linear σ model

The quantum dynamics of disordered single particle systems at long length- and time-scales is described by a diffusive non-linear σ model. The latter bears similarities to Ginzburg-Landau theories and encodes the physics of symmetry breaking and (critical) soft-mode fluctuations related to Anderson localization. Different from the former, the field degree of freedom of the σ model however does not afford the interpretation of an order parameter. More specifically, the model is formulated in terms of a matrix degree of freedom Q which satisfies the non-linear constraint $Q^2 = \mathbb{1}$. In its simplest replica variant the matrix is operating in a $2R$ -dimensional vector space formed by R replicas which exist in two “causal” variants, a “retarded” and an “advanced”. The replica structure helps to overcome the notorious problem of disorder averaging the logarithm of the partition function, which serves as a “generating function” for observables. The causal structure is introduced to generate the typical observables of interest (see Section II B in the main text), viz. disordered averaged probabilities (the product of retarded and advanced propagators), from a single generating function.

Anderson localization can be viewed as the restoration of rotational symmetry in causal space. Indeed, the derivation of the field theory builds around a saddle point that describes the disorder induced level broadening. This is isotropic in replica space, while causality breaks rotational symmetry in retarded and advanced components. Formally, $Q_0 \equiv \sigma_3 \otimes \mathbb{1}_R$ where σ_3 operates in causal space, and the soft mode action of the associated Goldstone modes $Q = TQ_0T^{-1}$ is precisely the diffusive non-linear sigma model, here restated for convenience of the reader

$$S_\sigma = \frac{1}{8} \sum_{i,j=1}^D \sigma_{ij}^{(0)} \int d^3x \text{Tr} (\partial_i Q \partial_j Q). \quad (\text{S1})$$

In the metallic regime, fluctuations around the saddle point are small. At the onset of localization, on the other hand, fluctuations grow uncontrolled and rotations start exploring the entire field manifold, restoring thus the original symmetry in causal space.

While the structure of S_σ is fixed by general principles, details of the matrix degree of freedom depend on the system’s symmetries. So far we have assumed the absence of fundamental symmetries. In the field theory construction fundamental symmetry are included by “symmetry doubling” of the matrix dimension. The effective description of a system with time reversal symmetry is e.g. in terms of a $4R$ dimensional matrix. Its entries are then constrained by a symmetry relation reminiscent of the symmetry doubling (see also Section S3 A). The same holds for other symmetries, that is, elements of the “symmetry doubled” matrices are not independent, and symmetry relations fix the field manifold to belong to one of ten symmetric spaces [42, 43].

B. Sketch of the derivation

A detailed derivation of the effective action S_σ for the dynamical protocol realizing the surface states of the $3d$ quantum spin Hall insulator can be found in Sections S3 A, S3 C, and S3 E, and we here only outline the basic steps (for the corresponding derivation for the quantum Hall simulator see e.g. the recent Ref. [28]). Starting out from the Floquet operator after gauge transformation,

$$\hat{U}_\Phi = \hat{U}_\mathbf{n} \hat{U}_\mathbf{k}, \quad (\text{S2})$$

we focus on the dynamics at long time and length scales. We assume that the action of the local disorder in physical space, $\hat{U}_\mathbf{n}$, in combination with the potential $\hat{\Phi}$, generated by the gauge transformation, induces non-integrability in all $1 + d_{\text{syn}}$ dimensions. This assumption is supported by the numerical simulations, as already discussed in the previous sections. To capture the universal long time dynamics, we may then erase system specific details introducing an ensemble of local spin rotations $U_\mathbf{n}$ (sharing fundamental symmetries of the system), and derive a generating functional for the *ensemble averaged* correlation function Eq. (8) in the main text.

For Floquet systems in class AII the derivation can be organized in terms of a color-flavor transformation (cft), whose details are exposed in Section S3 A. Its few line summary is as follows. Building on the replica trick and causal doubling, as discussed above, we lift the Floquet operator from a matrix operating in $2d$ spin space to a matrix $\hat{U}_\Phi \mapsto \hat{U}_\Phi \otimes \mathbb{1}_{2R}$, operating in the $2 \times 2 \times R$ dimensional product space of spin, causal and replica degrees of freedom. The cft then exchanges integrals over these local spin rotations, singlet in replica and causal space, for integrals over local rotations in replica and causal space, and structureless in spin-space. The latter conveniently accommodate the soft modes of the disordered system, viz. soft rotations in causal and replica space that are singlet in spin-space. Formally, the cft is an exact transformation which leads to an alternative representation of the generating functional in matrices that are the local

coordinates of the matrix degree of freedom $Q(\mathbf{n})$, discussed above. In a final step, see Section S3 C, the functional is expanded in slow fluctuations leading to a soft mode action $S = S_\sigma + S_{\text{top}}$, consisting of the non-linear diffusive σ model action and a topological term.

S2. FIELD THEORY OF CLASS A TOPOLOGICAL FLOQUET METAL

Nonlinear sigma models emerge as effective field theories, capturing the low energy sector of disordered single particle systems. For static quantum systems, the low energy sector usually describes a narrow window of energies around the Fermi level, relevant for the physics at long time and large distance scales. Effective field theories are then derived from averaging over disorder ensembles, usually in a Gaussian distribution. For time periodic quantum systems, on the other hand, a quasi-energy is defined only modulo $2\pi/T$. Disorder in these systems is usually modeled by random unitaries drawn from the Haar measure (respectively restrictions of the latter if symmetries are present), and there is no distinction between different quasi-energies. Zirnbauer [44] derived the nonlinear sigma model for time periodic quantum systems with random onsite unitary disorder using the color flavor transformation, and our discussion below is extensively based on this approach.

Once the effective field theory of a disordered system is known, one may naturally ask whether the system is subject to Anderson localization. By now it is well established that Anderson localization can be avoided if one of two topological terms, a \mathbb{Z}_2 topological term or a WZW term, is present. The possibility of the latter is determined by the system dimension and symmetries of the nonlinear sigma model target space [26]. Similarly, the existence of topological insulators and superconductors in a given dimension and symmetry class can be inferred from the presence of robust metallic boundary modes. These modes are not subject to Anderson localization and thus define a topological metal. In the present work we propose quantum simulators of single copies of topological metals, realized e.g. at the *isolated* surfaces of topologically non trivial insulators.

More specifically, d -dimensional systems in class A are eligible to topological metallic phases if $\pi_{d+1}(U(N+M)/U(N) \times U(M)) = \mathbb{Z}$. Notice here that target manifolds of nonlinear sigma models for Floquet and static systems within the same symmetry class are identical, and table 2 of Ryu *et al.* [26] applies for both. In our previous work [28] we derived the nonlinear sigma model action for a $2d$ class A Floquet system, composed of the conventional diffusive contribution and a Pruisken θ term. This system is subject to Anderson localization and flows (in the thermodynamic limit) to one of the \mathbb{Z} topological insulating phases of the Quantum Hall class. Its $1d$ boundary mode is chiral and topologically protected by the winding number of the $2d$ insulating bulk.

The effective theory describing the $1d$ boundary mode can be expressed as a product of the $1d$ winding number characterizing the chiral edge mode and a $(1+1)d$ WZW term, in which the matrix field of the $1d$ real space coordinate is deformed (by introduction of an additional homotopy parameter) into a trivial field configuration.

In the present work we derive the effective action for a $3d$ topological metal in class A. Its topological term is composed of a $3d$ winding number multiplied by $(3+1)d$ WZW term, in which the matrix field parametrized by the $3d$ real space coordinate is extended (by introduction of an additional homotopy parameter) to a trivial configuration. Since $\pi_4(U(N+M)/U(N) \times U(M)) = \mathbb{Z}$, the possibility of topologically nontrivial field configurations is guaranteed, however, as already discussed constructing a physical model with $3d$ winding number is not trivial. We here achieve such model employing the idea of synthetic dimensions engineered via time dependent protocols. The proposed model can be realized in a quantum walk setting, for example, using the optical network shown in Fig. 3 and discussed in the main text.

An alternative realization of a topological metal is via the emergence of a \mathbb{Z}_2 topological term in the effective field theory description. The latter also protects against Anderson localization, and can be realized in one of the real symmetry classes, for example, in a $2d$ class AII system for which $\pi_2(O(N+M)/O(N) \times O(M)) = \mathbb{Z}_2$. In Section D we derive the nonlinear sigma model for a time reversal symmetric Floquet system using the color flavor transformation. We verify that the \mathbb{Z}_2 topological term is written as the product of two $(2+1)d$ WZW terms of matrix fields, one involving the translational invariant part of the time evolution operator and the other the sigma model field degree of freedom. In combination with the \mathbb{Z} example, this completes our derivation of low energy effective field theories for topological Floquet metals, their model realizations, and numerical confirmation of the absence of Anderson localization.

In the remaining part of this Section we discuss the field theories for class A and class AII systems. We introduce the color flavor transformation for class A, and the derivation of a $(3+1)d$ WZW term is detailed in Section C. In Section D we present the color flavor transformation for class AII systems and the derivation of a \mathbb{Z}_2 topological term, and its alternative representation in terms of a WZW term.

A. Color-flavor transformation class A Floquet systems

Consider a Floquet system described by the single time step evolution operator \hat{U}_0 , to which onsite disorder is introduced by adding to the time evolution locally uncorrelated random phases. The microscopic action is then of the following general form, $Z = \int D(\psi, \bar{\psi}) \exp(-S)$,

with

$$S = \int d^d \mathbf{x} \bar{\psi}_{\mathbf{x}}^{+a} (\hat{G}_+^{-1})_{\mathbf{x}\mathbf{x}'} \psi_{\mathbf{x}'}^{+a} + \bar{\psi}_{\mathbf{x}}^{-a} (\hat{G}_-^{-1})_{\mathbf{x}\mathbf{x}'} \psi_{\mathbf{x}'}^{-a}, \quad (\text{S1})$$

$$(\hat{G}_+^{-1})_{\mathbf{x}\mathbf{x}'} = \delta_{\mathbf{x}\mathbf{x}'} - e^{i\phi_{\mathbf{x}}} (\hat{U}_0)_{\mathbf{x}\mathbf{x}'}, \quad (\text{S2})$$

$$(\hat{G}_-^{-1})_{\mathbf{x}\mathbf{x}'} = \delta_{\mathbf{x}\mathbf{x}'} - (\hat{U}_0^\dagger)_{\mathbf{x}\mathbf{x}'} e^{-i\phi_{\mathbf{x}'}} \quad (\text{S3})$$

where $\exp(i\phi_{\mathbf{x}})$ are the uniformly distributed phases, and ‘ a ’ carries spin, replica, and particle-hole indices. Upon introduction of adequate source terms (see e.g. Ref. [28] for details), Eq. (S1) allows for the convenient generation of products $\langle G^+ G^- \rangle$, e.g. required for the calculation of Eq. (8) in the main text. The disorder averaging of the generating function $\langle Z \rangle = \prod_{\mathbf{x}} \frac{1}{2\pi} \int d\phi_{\mathbf{x}} Z(\{\phi_{\mathbf{x}}\})$ is performed by the color flavor transformation:

$$\frac{1}{2\pi} \int d\phi_{\mathbf{x}} e^{\bar{\psi}_{\mathbf{x}}^{+a} e^{i\phi_{\mathbf{x}}} \varphi_{\mathbf{x}}^{+a} + \bar{\varphi}_{\mathbf{x}}^{-a} e^{-i\phi_{\mathbf{x}}} \psi_{\mathbf{x}}^{-a}} \quad (\text{S4})$$

$$= \int D(Z_{\mathbf{x}}, \tilde{Z}_{\mathbf{x}}) e^{-\text{tr} \ln(1 - \tilde{Z}_{\mathbf{x}} Z_{\mathbf{x}})} e^{\bar{\psi}_{\mathbf{x}}^{+a} Z_{\mathbf{x}}^{ab} \psi_{\mathbf{x}}^{-b} + \bar{\varphi}_{\mathbf{x}}^{-a} \tilde{Z}_{\mathbf{x}}^{ab} \varphi_{\mathbf{x}}^{+b}}, \quad (\text{S5})$$

applying for every position \mathbf{x} . Here the Floquet operator \hat{U}_0 has been absorbed into the newly defined Grassmann fields $\varphi_{\mathbf{x}}^{+a} = (\hat{U}_0 \psi)_{\mathbf{x}}^{+a}$ and $\bar{\varphi}_{\mathbf{x}}^{-a} = (\bar{\psi} \hat{U}_0^\dagger)_{\mathbf{x}}^{-a}$, and the domain of integration is defined by the condition $\tilde{Z} = -Z^\dagger$. The matrix field $Z_{\mathbf{x}}^{ab}$ connects retarded (+) and advanced (-) Grassmann field, indicating that its spatial fluctuation encodes diffusion in the long distance limit. Its role becomes more clear by introducing $Q = T\tau_3 T^{-1}$ with

$$T \equiv \begin{pmatrix} \mathbb{1} & Z \\ \tilde{Z} & \mathbb{1} \end{pmatrix}_{\text{RA}},$$

and anticipating that the effective field theory is expressed in terms of the matrix field Q with nonlinear constraint $Q^2 = \mathbb{1}$. More specifically, Z defines linear coordinates on the symmetric space $U(2R)/U(R) \times U(R)$ with $Z = 0$ representing the ‘north pole’, $Q = \tau_3$, and $Z \rightarrow \infty$ the ‘south pole’, $Q = -\tau_3$. After integration over Grassman fields, we obtain the class A action entirely expressed in terms of the linear coordinates,

$$S[Z, \tilde{Z}] = -\text{tr} \ln(1 - \tilde{Z}Z) + \text{tr} \ln(1 - \tilde{Z}UZU^\dagger).$$

In Ref.[28] we derived the low energy effective action of a 2d Floquet topological insulator, composed of the conventional diffusive term accompanied by a Pruisken θ term. This allowed us to confirm that the maximally disordered Floquet system belongs to the integer quantum Hall universality class. In the following sections, we derive the effective theory for a 3d Floquet system. This turns out to contain a Chern-Simons action, and thus is within the same universality class as Weyl semimetals without intervalley scattering.

B. Soft-mode actions for class A

A straightforward manipulation of block matrices brings the above representation of the action into the

form [28]

$$S = \frac{1}{2} \sum_{s=\pm} \text{Tr} \ln(1 + X_s P^s), \quad (\text{S6})$$

$$X_- \equiv \hat{T}^{-1} [\hat{U}_0, \hat{T}] \hat{U}_0^\dagger, \quad X_+ \equiv \hat{T}^{-1} [\hat{U}_0^\dagger, \hat{T}] \hat{U}_0, \quad (\text{S7})$$

where $P^\pm = (\mathbb{1} \pm \tau_3)/2$ are projectors onto retarded and advanced sectors of the theory. To simplify notation, we will in the following drop the index ‘0’ of the Floquet operator \hat{U}_0 . An expansion of the log-function to the third order is necessary,

$$S = S^{(1)} + S^{(2)} + S^{(3)}, \quad (\text{S8})$$

where

$$S^{(1)} = \frac{1}{2} \sum_{s=\pm} \text{Tr}(X_s P^s),$$

$$S^{(2)} = -\frac{1}{4} \sum_{s=\pm} \text{Tr}((X_s P^s)^2),$$

$$S^{(3)} = \frac{1}{6} \sum_{s=\pm} \text{Tr}((X_s P^s)^3).$$

In the following sections, using the Wigner transformation the continuum representation of the action is obtained.

1. The first order terms $S^{(1)}$

Consider the ‘-’ contribution to the action $S^{(1)}$,

$$\begin{aligned} S^{(1)-} &= \frac{1}{2} \text{Tr} \left((\hat{T}^{-1} \hat{U} \hat{T} \hat{U}^\dagger - \mathbb{1}) P^- \right), \\ &= \frac{1}{2} \text{Tr} \left(\int_0^t ds (\hat{T}^{-1} \partial_s \hat{U} \hat{T} \hat{U}^\dagger + \hat{T}^{-1} \hat{U} \hat{T} \partial_s \hat{U}^\dagger) P^- \right), \\ &= \frac{1}{2} \int_0^t ds \text{Tr} \left(([\hat{T}^{-1}, \partial_s \hat{U} \hat{U}^\dagger] \hat{U} \hat{T} \hat{U}^\dagger) P^- \right), \\ &= -\frac{1}{2} \int_0^t ds \text{Tr} \left(([\hat{T}^{-1}, \hat{\psi}_s^-] [\hat{U}, \hat{T}] \hat{U}^\dagger + [\hat{T}^{-1}, \hat{\psi}_s^-] \hat{T}) P^- \right), \end{aligned}$$

where in the third equality $\hat{U} \partial_s \hat{U}^\dagger = -\partial_s \hat{U} \hat{U}^\dagger \equiv \hat{\psi}_s^-$ is used. Note that \hat{U} has no structure in replica space, thus $[\partial_s \hat{U}^\dagger, P^-] = 0$ is used. The commutator in the third line can be Moyal expanded up to the third derivatives,

$$[\hat{T}^{-1}, \hat{\psi}_s^-] [\hat{U}, \hat{T}] \hat{U}^\dagger \simeq (\partial_i T^{-1} \partial_i \hat{\psi}_s^-) (\partial_j U \partial_j T U^\dagger),$$

and

$$[\hat{T}^{-1}, \hat{\psi}_s^-] \hat{T} \simeq i(\partial_i T^{-1} \partial_i \hat{\psi}_s^-) T - \frac{i}{24} (\partial_{ijk}^3 \hat{\psi}_s^- \partial_{ijk}^3 T^{-1}) T,$$

where distinction between an operator and a function is made by hat on symbols. $\partial_i U \equiv \partial_{k_i} U$ and $\partial_i T \equiv$

$\partial_{x_i} T$ and sum over index i, j, k is implicitly assumed. By plugging in the above into the action,

$$\begin{aligned} S^{(1)-} = & -\frac{i}{2} \int_0^t ds \operatorname{Tr} ((\partial_i T^{-1} T)(\partial_i \psi_s^-) P^-) \\ & + \frac{1}{2} \int_0^t ds \operatorname{Tr} ((\partial_i T^{-1} \partial_j T)(\partial_i \psi_s^- \psi_j^-) P^-) \\ & + \frac{i}{48} \int_0^t ds \operatorname{Tr} ((\partial_{ijk}^3 T^{-1} T)(\partial_{ijk}^3 \psi_s^-) P^-), \end{aligned}$$

where the first and third term vanish after the momentum integration because ψ_s^- is a periodic function in momentum. The second term, which is obtained using $\partial_j U U^\dagger = -U \partial_j U^\dagger = -\psi_j^-$, is,

$$S_{2\text{nd}}^{(1)-} = \frac{1}{2} \int_0^t ds \operatorname{Tr} (\partial_i T^{-1} \partial_j T P^-) \operatorname{tr} (\partial_i \psi_s^- \psi_j^-). \quad (\text{S9})$$

Eq. (S9) is identical to the one in [28], from which the Pruisen action and a part of diffusive action is derived.

2. The second order terms $S^{(2)}$

Using $X_- = \hat{T}^{-1}[\hat{U}, \hat{T}]\hat{U}^\dagger = \hat{T}^{-1}\hat{U}[\hat{T}, \hat{U}^\dagger] \rightarrow i(T^{-1} * U) * \partial_i T \partial_i U^\dagger$, and Moyal expand to the third derivatives,

$$\begin{aligned} (T^{-1} * U) * \partial_i T \partial_i U^\dagger & \simeq T^{-1} U \partial_i T \partial_i U^\dagger + \frac{i}{2} (\partial_k T^{-1} \partial_k U) \partial_i T \partial_i U^\dagger \\ & + \frac{i}{2} (\partial_k T^{-1} U) \partial_i T \partial_{ik}^2 U^\dagger - \frac{i}{2} (T^{-1} \partial_k U) \partial_{ik}^2 T \partial_i U^\dagger, \end{aligned}$$

which is then plug in to $S^{(2)-}$,

$$\begin{aligned} S^{(2)-} = & \frac{1}{4} \operatorname{Tr} ((T^{-1} \partial_i T) P^- (T^{-1} \partial_j T) P^- (U \partial_i U^\dagger U \partial_j U^\dagger)) \\ & + \frac{i\epsilon^{ijk}}{4} \operatorname{Tr} ((\partial_k T^{-1} \partial_i T) P^- (T^{-1} \partial_j T) P^- (\partial_k U \partial_i U^\dagger U \partial_j U^\dagger)) \\ & + \frac{i\epsilon^{ijk}}{4} \operatorname{Tr} ((\partial_k T^{-1} \partial_i T) P^- (T^{-1} \partial_j T) P^- (U \partial_{ik}^2 U^\dagger U \partial_j U^\dagger)) \\ & - \frac{i\epsilon^{ijk}}{4} \operatorname{Tdr} ((T^{-1} \partial_{ik}^2 T) P^- (T^{-1} \partial_j T) P^- (\partial_k U \partial_i U^\dagger U \partial_j U^\dagger)). \end{aligned} \quad (\text{S10})$$

The Levi-Civita symbol is introduced because only anti-symmetric combinations are nonzero for the 3-dim TFM unitary operator. Thus, the third and fourth term in (S10) is zero. Introducing $A_i = T^{-1} \partial_i T$,

$$\begin{aligned} S^{(2)-} = & \frac{1}{4} \operatorname{Tr} ((A_i P^- A_j P^-) (\psi_i^- \psi_j^-)) \\ & + \frac{i}{4} \epsilon^{ijk} \operatorname{Tr} ((A_k A_i P^- A_j P^-) (\psi_k^- \psi_i^- \psi_j^-)), \end{aligned}$$

Note that $\epsilon^{ijk} A_j A_k = -\epsilon^{ijk} \partial_j A_k$. On the other hand,

$$\begin{aligned} S^{(2)+} = & \frac{1}{4} \operatorname{Tr} ((A_i P^+ A_j P^+) (\psi_i^+ \psi_j^+)) \\ & + \frac{i}{4} \epsilon^{ijk} \operatorname{Tr} ((A_k A_i P^+ A_j P^+) (\psi_k^+ \psi_i^+ \psi_j^+)). \end{aligned}$$

Employing that $\operatorname{tr}(\psi_i^+ \psi_j^+) = \operatorname{tr}(\psi_i^- \psi_j^-)$ and $\operatorname{tr}(\psi_i^+ \psi_j^+ \psi_k^+) = -\operatorname{tr}(\psi_i^- \psi_j^- \psi_k^-)$, the latter two terms of $S^{(2)\pm}$ can be combined as

$$\begin{aligned} S^{(2)} = & \frac{1}{4} \sum_{s=\pm} \operatorname{Tr} (A_i P^s A_j P^s) \quad (\text{S11}) \\ & - \frac{i\epsilon^{ijk}}{4} \sum_{s=\pm} s \operatorname{Tr} (\partial_k A_i P^s A_j P^s) \operatorname{tr} (\psi_i^+ \psi_j^+ \psi_k^+), \end{aligned}$$

where the first term becomes part of the diffusive action (see Eq.(30) of Ref. [28]), and the second term constitutes the first part of the Chern-Simons action.

3. The third order terms $S^{(3)}$

The third order expansion of the log yields,

$$\begin{aligned} S^{(3)-} = & \frac{i^3}{6} \epsilon^{ijk} \operatorname{Tr} ((T^{-1} U \partial_i T \partial_i U^\dagger) P^- \\ & \times (T^{-1} U \partial_j T \partial_j U^\dagger) P^- (T^{-1} U \partial_k T \partial_k U^\dagger) P^-), \\ = & -\frac{i}{6} \epsilon^{ijk} \operatorname{Tr} (A_i P^- A_j P^- A_k P^-) \operatorname{tr} (\psi_i^- \psi_j^- \psi_k^-), \end{aligned}$$

and similarly,

$$S^{(3)+} = -\frac{i}{6} \epsilon^{ijk} \operatorname{Tr} (A_i P^+ A_j P^+ A_k P^+) \operatorname{tr} (\psi_i^+ \psi_j^+ \psi_k^+).$$

Combining the latter with the 2nd piece in Eq. (S11), we arrive at

$$S^{(3)} = -\frac{i\epsilon^{ijk}}{6} \sum_{s=\pm} s \operatorname{Tr} (A_i P^s A_j P^s A_k P^s) \operatorname{tr} (\psi_i^+ \psi_j^+ \psi_k^+),$$

which constitutes the second part of the Chern-Simons action. Introducing the winding number $\nu_3 = \frac{1}{24\pi^2} \int d^3 k \epsilon^{\mu\nu\rho} \operatorname{tr} (\psi_\mu^+ \psi_\nu^+ \psi_\rho^+)$, the Chern-Simons action can be expressed in the following form:

$$S_{\text{top}} = \nu_3 \int_{\partial B_4} (w_{\text{CS}}[AP^+] - w_{\text{CS}}[AP^-]),$$

where $w_{\text{CS}}[A] = \frac{i}{8\pi} (A \wedge dA + \frac{2}{3} A \wedge A \wedge A)$. As a result we obtain the topological action summarized in Eqs. (23) and (25) in the main text. Notice that the presence of the Chern-Simons action can be anticipated for a 3d class A system, noting that the homotopy group $\pi_{3+1}(U(2R)/U(R) \times U(R)) = \mathbb{Z}$ is nontrivial. That is, the field $T = T(\mathbf{x})$ can be extended from 3d space to the matrix field $Q = Q(x_0, \mathbf{x})$ in one dimension higher, and the topological action can then be expressed as a WZW term (see Ref. [36]):

$$S_{\text{top}} = \frac{i\nu_3}{128\pi} \int_{B_4} \operatorname{Tr} [Q(\wedge dQ)^4].$$

S3. FIELD THEORY OF CLASS AII TOPOLOGICAL FLOQUET METAL

In this Section we provide details on the effective field theory for class AII Floquet systems. We first present the color flavor transformation for the latter, from which the disorder averaged effective action is derived in D.1. The softmode manifold of class AII systems is specified in D.2, and in sections D.3 and D.4 we present the non-linear sigma model composed of a diffusive and a topological term. The latter is expressed as the product of two WZW terms, measuring the topological content of mappings from momentum and real space, respectively. We provide the connection of the topological term and the color flavor action in D.5, completing thus the derivation of effective field theories for Floquet topological metals. Conventions used throughout the sections are as follows. We use symbols σ_j to indicate sublattice space, τ_j for retarded-advanced space, and s_j for particle-hole space. Vectors $(x_0, \mathbf{x}) = (x_0, x_1, \dots, x_d)$ summarize the spatial coordinate and homotopy parameter, and correspondingly, $(k_0, \mathbf{k}) = (k_0, k_1, \dots, k_d)$, for momentum coordinates including a homotopy parameter.

A. Color-flavor transformation for class AII Floquet systems

We recall that the 2×2 dimensional time evolution operator in class AII satisfies the time-reversal symmetry constraint $\sigma_2 \mathcal{U}_{\mathcal{F}}^T \sigma_2 = \mathcal{U}_{\mathcal{F}}$. It can be written as a product

$$\mathcal{U}_{\mathcal{F}} = V U_0 \bar{V}, \quad \bar{V} = \sigma_2 V^T \sigma_2, \quad \bar{U}_0 = \sigma_2 U_0^T \sigma_2 \equiv U_0, \quad (\text{S1})$$

where U_0 is a non-random part while V and \bar{V} encode the unitary disorder. For the simplicity of notation the index zero in the clean part of the Floquet operator U_0 will be dropped in the following discussion. Concentrating e.g. on the contribution of the retarded (+) sector to the action (S1), the above decomposition of $\mathcal{U}_{\mathcal{F}}$ allows to rewrite

$$S_+ = \bar{\psi}_{+1} \psi_{+1} + \bar{\psi}_{+2} \psi_{+2} - \bar{\psi}_{+1} e^{i\phi_+} V \psi_{+2} - \bar{\psi}_{+2} U \bar{V} \psi_{+1}, \quad (\text{S2})$$

where we introduced the two-component spinor $\bar{\psi}_+ = (\bar{\psi}_{+1}, \bar{\psi}_{+2})$ and similar for ψ_+ . A constant source term ϕ_+ is introduced. We then arrange contributions containing \bar{V} using time reversal symmetry,

$$\begin{aligned} \bar{\psi}_{+2} U \bar{V} \psi_{+1} &= (\bar{\psi}_{+2} U \sigma_2 V^T \sigma_2 \psi_{+1})^T \\ &= -\psi_{+1}^T \sigma_2 V \sigma_2 U^T \bar{V} \bar{\psi}_{+2}^T \\ &= -(\psi_{+1}^T \sigma_2) V (U \sigma_2 \bar{\psi}_{+2}^T), \end{aligned} \quad (\text{S3})$$

and upon introducing spinors

$$\varphi_+^T = (\bar{\psi}_{+1}, i \psi_{+1}^T \sigma_2), \quad \chi_+ = \begin{pmatrix} e^{i\phi_+} \psi_{+2} \\ U i \sigma_2 \bar{\psi}_{+2}^T \end{pmatrix}, \quad (\text{S4})$$

we can cast this action into the simpler form

$$S_+ = \bar{\psi}_{+1} \psi_{+1} + \bar{\psi}_{+2} \psi_{+2} - \varphi_+^T V \chi_+. \quad (\text{S5})$$

Proceeding along the same lines for the contribution of the advanced sector to the action (S1),

$$S_- = \bar{\psi}_{-1} \psi_{-1} + \bar{\psi}_{-2} \psi_{-2} - \bar{\psi}_{-1} \bar{V}^\dagger U^\dagger \psi_{-2} - \bar{\psi}_{-2} V^\dagger e^{-i\phi_-} \psi_{-1}, \quad (\text{S6})$$

the disorder term $\propto V^\dagger$ can be reorganized employing time reversal symmetry,

$$\begin{aligned} \bar{\psi}_{-1} \bar{V}^\dagger U^\dagger \psi_{-2} &= (\bar{\psi}_{-1} \sigma_2 V^* \sigma_2 U^\dagger \psi_{-2})^T \\ &= -(\psi_{-2}^T U^* \sigma_2) V^\dagger (\sigma_2 \bar{\psi}_{-1}) \\ &= -(\psi_{-2}^T \sigma_2 U^\dagger) V^\dagger (\sigma_2 \bar{\psi}_{-1}) \end{aligned} \quad (\text{S7})$$

and upon introducing the spinors

$$\chi_-^T = (\bar{\psi}_{-2} e^{-i\phi_-}, i \psi_{-2}^T \sigma_2 U^\dagger), \quad \varphi_- = \begin{pmatrix} \psi_{-1} \\ i \sigma_2 \bar{\psi}_{-1}^T \end{pmatrix}, \quad (\text{S8})$$

into the form

$$S_- = \bar{\psi}_{-1} \psi_{-1} + \bar{\psi}_{-2} \psi_{-2} - \chi_-^T V^\dagger \varphi_-. \quad (\text{S9})$$

With these preparations we can now apply the color-flavor transformation to the action $S = S_+ + S_-$ by averaging over V using (S5). This amounts to exchanging matrices V, V^\dagger , with structure in spin space, for matrices Z, \tilde{Z} , with structure in replica and causal space. That is,

$$\begin{aligned} S_1 &= \bar{\psi}_{+1} \psi_{+1} + \bar{\psi}_{-1} \psi_{-1} - \varphi_+^T Z \varphi_-, \\ S_2 &= \bar{\psi}_{+2} \psi_{+2} + \bar{\psi}_{-2} \psi_{-2} - \chi_-^T \tilde{Z} \chi_+, \end{aligned} \quad (\text{S10})$$

and we notice that $\psi_{\pm 1}$ can be expressed entirely in terms of φ_{\pm} , and correspondingly, $\psi_{\pm 2}$ entirely in terms of χ_{\pm} . The subsequent path integral can therefore be split into two independent integrals over φ and χ with actions S_1 and S_2 , respectively.

To proceed, we organize \pm indices of vectors φ and χ into a two dimensional space, in the following referred to as ‘particle-hole (ph)’ space, and introduce the matrix $s_1 \equiv \sigma_1^{\text{ph}}$, operating in this space, with $s_1^T s_1 = 1$. We then notice that

$$\begin{aligned} \varphi_+^T (i \sigma_2 \otimes s_1) \varphi_+ &= 2 \bar{\psi}_{+1} \psi_{+1}, \\ \varphi_-^T (i \sigma_2 \otimes s_1) \varphi_- &= 2 \bar{\psi}_{-1} \psi_{-1}, \\ \chi_+^T e^{-i\phi_+} (i \sigma_2 \otimes s_1) U^\dagger \chi_+ &= 2 \bar{\psi}_{+2} \psi_{+2}, \\ \chi_-^T e^{i\phi_-} (i \sigma_2 \otimes s_1) U^T \chi_- &= 2 \bar{\psi}_{-2} \psi_{-2}, \end{aligned} \quad (\text{S11})$$

which allows us to express actions $S_{1,2}$ in the form

$$S_1 = \frac{1}{2} (\varphi_+^T, \varphi_-^T) \begin{pmatrix} (i \sigma_2 \otimes s_1) & -Z \\ Z^T & (i \sigma_2 \otimes s_1) \end{pmatrix} \begin{pmatrix} \varphi_+ \\ \varphi_- \end{pmatrix}, \quad (\text{S12})$$

and

$$S_2 = \frac{1}{2}(\chi_+^T, \chi_-^T) \times \begin{pmatrix} e^{-i\phi_+}(i\sigma_2 \otimes s_1)U^\dagger & \tilde{Z}^T \\ -\tilde{Z} & e^{i\phi_-}(i\sigma_2 \otimes s_1)U^T \end{pmatrix} \begin{pmatrix} \chi_+ \\ \chi_- \end{pmatrix},$$

where we used that $\varphi_+^T Z \varphi_- = -\varphi_-^T Z^T \varphi_+$ and similar for χ . In a final step we then complete Gaussian integrals over φ and χ . Accounting for a nontrivial Jacobian $J(\phi_+, \phi_-) = (e^{-i(\phi_+ - \phi_-)})^{-1}$ resulting from the change of integration variables, we arrive at

$$\mathcal{Z} \propto J(\phi_+, \phi_-) \det^{1/2} \begin{pmatrix} i\sigma_2 \otimes s_1 & -Z \\ Z^T & i\sigma_2 \otimes s_1 \end{pmatrix} \times \det^{1/2} \begin{pmatrix} e^{-i\phi_+}(i\sigma_2 \otimes s_1)U^\dagger & \tilde{Z}^T \\ -\tilde{Z} & e^{i\phi_-}(i\sigma_2 \otimes s_1)U^T \end{pmatrix}. \quad (\text{S13})$$

Finally, restoring the measure $\mu(Z, \tilde{Z}) = \det(1 - \tilde{Z}Z)^{-1}$ of the color-flavor transformation, we arrive at $\mathcal{Z} = e^S$, with

$$S = -\text{tr} \ln(1 - \tilde{Z}Z) + \frac{1}{2} \text{tr} \ln(1 - Z^T s_1 Z s_1^T) + \frac{1}{2} \text{tr} \ln(1 - \tilde{Z}U s_1^T e^{i\phi_+} \tilde{Z}^T e^{-i\phi_-} s_1 U^\dagger). \quad (\text{S14})$$

Upon color-flavor transformation (enabling the disorder averaging), the original action for ‘microscopic’ Grassmann fields is expressed in terms of the matrix fields Z, \tilde{Z} . These are more convenient to extract the low energy content of the theory, and to access the low energies we subject the action to a saddle point analysis. Allowing for (soft) spatial fluctuations around the saddle points we then derive the low energy effective action. We notice that the target space of the matrix field is topologically non trivial and the generating function must include the sum over topologically distinct configurations, weighting topologically different sectors by a topological contribution to the action. We present the effective action in Sections S3 C and S3 D, and the derivation of the topological term (starting out from Eq.(S14)) in Sec.S3 E.

B. Soft-mode manifold for class AII

We then notice that in the zero frequency limit, $\phi_\pm \rightarrow 0$, action Eq. (S14) is minimized by homogeneous configurations Z, \tilde{Z} related via

$$\tilde{Z} = s_1^T Z^T s_1. \quad (\text{S15})$$

The soft mode action reads

$$S[Z, \tilde{Z}] = -\frac{1}{2} \text{tr} \ln(1 - \tilde{Z}Z) + \frac{1}{2} \text{tr} \ln(1 - \tilde{Z}U Z U^\dagger), \quad (\text{S16})$$

which apart from the factor 1/2 and symmetry constraint Eq. (S15), is the same as that encountered for class A

systems. (See e.g. Ref. [28] for a discussion in the context of the above mentioned AFAI.)

To further elaborate on the soft mode manifold, we introduce matrices, $\tau_3 \equiv \sigma_3^{\text{RA}}$,

$$Q = T\tau_3 T^{-1}, \quad T = \begin{pmatrix} 1 & Z \\ \tilde{Z} & 1 \end{pmatrix}_{\text{RA}}, \quad (\text{S17})$$

satisfying the symmetry constraint [34]

$$\bar{Q} = Q, \quad \bar{Q} \equiv C^T Q^T C, \quad C = \tau_3 \otimes s_1. \quad (\text{S18})$$

The explicit expression for the Q -matrix read,

$$Q = \begin{pmatrix} \frac{1+Z\tilde{Z}}{1-Z\tilde{Z}} & -2Z\frac{1}{1-\tilde{Z}Z} \\ 2\tilde{Z}\frac{1}{1-\tilde{Z}Z} & -\frac{1+\tilde{Z}Z}{1-\tilde{Z}Z} \end{pmatrix}_{\text{RA}}, \quad (\text{S19})$$

where we recall the relation $A(1-BA)^{-1} = (1-AB)^{-1}A$. One can now verify that owing to (S15) the relation $C^T Q^T C = Q$ holds. This defines the soft mode manifold of class AII systems.

C. Soft-mode actions for class AII

Following the steps discussed in Ref. [28], we can apply a gradient expansion to derive a diffusive σ model action for Q fields. The non trivial properties of the dynamical protocols for the simulators of topological surface states are encoded in an additional topological contribution to the soft mode action. Their derivation is discussed in more detail below. The soft mode action for Q -matrix fields satisfying AII symmetry constraint $Q = \bar{Q}$ therefore reads $S = S_\sigma + S_{\text{top}}$, where

$$S_\sigma[Q] = -\frac{1}{8} \sum_{i,j=1}^2 \sigma_{ij}^{(0)} \int d^2x \text{tr}(\partial_i Q \partial_j Q), \quad (\text{S20})$$

$$S_{\text{top}}[Q] = \frac{i\theta}{\pi} \Gamma[g] \Big|_{g(x_0=0, \mathbf{x})=Q(\mathbf{x})}, \quad (\text{S21})$$

with conductivity tensor $\sigma_{ij}^{(0)} = \frac{1}{2} \int d^2\mathbf{k} \text{tr}(\partial_{k_i} U_{\mathbf{k}} \partial_{k_j} U_{\mathbf{k}}^{-1})$ and topological angle, $\theta = 0, \pi$ defined in Eq. (S26). $\Gamma[g]$ in Eq. (S21) is a WZW functional

$$\Gamma[g] = \frac{1}{24\pi} \int_0^1 dx_0 \int d^2\mathbf{x} \epsilon^{\mu\nu\rho} \text{tr} (g^{-1} \partial_\mu g g^{-1} \partial_\nu g g^{-1} \partial_\rho g), \quad (\text{S22})$$

here defined for matrices g from the orthogonal group $O(4R)$, satisfying the symmetry relation $\bar{g} = C^T g^T C = g^{-1}$, and with constraint $g(x_0 = 1, \mathbf{x}) = \tau_3$.

Several comments are here of order. (i) We remind that the WZW action depends only on the boundary value of the group field, $g(x_0 = 0, \mathbf{x})$. Given that the homotopy group $\pi_2(O(4R)) = 0$ is trivial, an extension to the third dimension x_0 with constant boundary value at $x_0 = 1$

is always possible. (ii) As we show below, $\Gamma[g]$ is only defined modulo π . However, recalling that $\theta = 0, \pi$, the exponentiated action $e^{-S_{\text{top}}[Q]} = \pm 1$ is well defined. (iii) Finally, as already discussed in the main text, the possibility to add the topological term $S_{\text{top}}[Q]$ to the diffusive action is related to the nontrivial homotopy group of the coset space, $\pi_2(\text{O}(4R)/\text{O}(2R) \times \text{O}(2R)) = \mathbb{Z}_2$.

We conclude our discussion, showing that $S_{\text{top}}[Q]$ is indeed a \mathbb{Z}_2 topological term. That is, it (a) does not change under local variations of Q which stay in the same equivalence class, and (b) takes values 0 or $i\pi$. Starting out with (a), we first notice that variation of the WZW action with respect to arbitrary fluctuations g gives

$$\delta\Gamma[g] = \frac{1}{8\pi} \int d^2\mathbf{x} \epsilon^{\mu\nu} \text{tr}(g^{-1} \delta g g^{-1} \partial_\mu g g^{-1} \partial_\nu g) \Big|_{x_0=0}. \quad (\text{S23})$$

Recalling then that on the coset manifold $Q^{-1} = Q$, we can use $Q\delta Q = -\delta Q Q$ and $Q\partial_\mu Q = -\partial_\mu Q Q$, to find

$$\begin{aligned} \epsilon^{\mu\nu} \text{tr}(Q\delta Q Q\partial_\mu Q Q\partial_\nu Q) \\ = -\epsilon^{\mu\nu} \text{tr}(\delta Q Q Q\partial_\mu Q Q\partial_\nu Q) \\ = -\epsilon^{\mu\nu} \text{tr}(Q\delta Q Q\partial_\mu Q Q\partial_\nu Q) = 0. \end{aligned} \quad (\text{S24})$$

That is, $\delta S_{\text{top}}[Q] = 0$ for any local variations of the Q -matrix. For (b), we show that $\Gamma[Q] = 0, \pi$ modulo contributions 2π . To this end, we extend $g(x_0 > 0, \mathbf{x})$ to $x_0 \in [-1, 0)$ defining $g(x_0 < 0, \mathbf{x}) = \bar{g}(x_0 > 0, \mathbf{x})$ which, recalling that $g|_{x_0=0} = Q = \bar{Q}$, is continuous at $x_0 = 0$. Denoting then by $\Gamma_+[g]$ and $\Gamma_-[g]$ the two WZW terms in Eq. (S22) for which integration over u is carried out over positive and negative values, respectively, (b) follows from the following two observations. First, $\Gamma_+[g] + \Gamma_-[g] = 2\pi\mathbb{Z}$ is counting the winding number of the orthogonal group (which reflects the non-trivial homotopy $\pi_3(\text{O}(4n)) = \mathbb{Z}$), and second, $\Gamma_+[g] = \Gamma_-[g]$. To show the latter, we notice that for $x_0 > 0$ we can write $g'(-x_0) = -\partial_{x_0} g(-x_0) = -\bar{g}'(x_0)$, and therefore

$$\begin{aligned} \Gamma_-[g] \\ = \frac{1}{24\pi} \int_{-1}^0 dx_0 \int d^2\mathbf{x} \epsilon^{\mu\nu\rho} \text{tr}(g^{-1} \partial_\mu g g^{-1} \partial_\nu g g^{-1} \partial_\rho g) \\ = -\frac{1}{24\pi} \int_0^1 dx_0 \int d^2\mathbf{x} \epsilon^{\mu\nu\rho} \text{tr}(\bar{g}^{-1} \partial_\mu \bar{g} \bar{g}^{-1} \partial_\nu \bar{g} \bar{g}^{-1} \partial_\rho \bar{g}) \\ = -\Gamma_+[g^{-1}] = \Gamma_+[g], \end{aligned} \quad (\text{S25})$$

where in the second line we set $x_0 \rightarrow -x_0$, and in the third line $\bar{g} = g^{-1}$. The value $\Gamma[g] = 0, \pi$ can be thought as the \mathbb{Z}_2 topological index of a matrix $Q = g(x_0 = 0, \mathbf{x})$, and is a direct analog of the winding number defined by the Pruisken action in the integer quantum Hall system.

D. \mathbb{Z}_2 index from “half” Wess-Zumino-Witten term

The alternative formulation of the \mathbb{Z}_2 index borrows concepts from the construction of topological Wess-Zumino-Witten (WZW) actions. It builds on a continuous deformation of the mapping $U_{\mathbf{k}}$ to the constant

matrix σ_2 . Generally, such deformation can only be found if one relaxes the original symmetry constraint, and allows the latter to leave the coset space and belong to the larger unitary group. Being simply connected, the unitary group leaves enough room for an interpolation, and indeed, for topologically nontrivial mappings the interpolation will violate time-reversal symmetry of the two-dimensional map at some fixed deformation parameter. We thus introduce the deformation $g_U(k_0, \mathbf{k})$ with $g_U(0, \mathbf{k}) = U_{\mathbf{k}}$ and $g_U(\pi, \mathbf{k}) = \sigma_2$, where different symbols are used to recall that the latter belongs to the coset space while the former to the full group. We can then extend the deformation to a mapping from the 3-torus to the coset $\text{U}(2)/\text{Sp}(2)$, by imposing time reversal symmetry on the three-dimensional map, $g_U(k_0, \mathbf{k}) = \sigma_2 g_U^T(-k_0, -\mathbf{k}) \sigma_2$. This mapping can now be characterized by a winding number. The crucial observation then is that by construction (viz. time-reversal symmetry) integrals over positive and negative half tori, $-\pi \leq k_0 \leq 0$ and $0 \leq k_0 \leq \pi$ respectively, contribute equally to the winding. One may thus define the θ angle as 2π multiplied by half-winding number,

$$\theta[U_{\mathbf{k}}] = \frac{1}{12\pi} \int_{\mathcal{M}} \text{tr}(\Phi_U \wedge \Phi_U \wedge \Phi_U) \bmod 2\pi, \quad (\text{S26})$$

where $\Phi_U = g_U^{-1} dg_U$ and the integral here is over the half 3-torus $\mathcal{M} = [0, \pi] \times [-\pi, \pi]^2$. Notice however, that being constructed from a WZW action it only depends on the boundary value, i.e. modulo 2π it is uniquely fixed by the original map $U_{\mathbf{k}}$. Eq. (S26) takes values 0 or π and we verify explicitly in Sections S3 D that for the dynamical protocol realizing $\text{FM}_{1+1_{\text{syn}}}$ it leads to the result Eq. (22).

We can now extend the above construction to introduce a topological action for the field mapping Eq. (33). Following the above procedure we introduce a deformation of the original mapping to $\tau_3 \otimes \mathbb{1}_{2R}$, i.e. $g(x_0, \mathbf{x})$ with $g(0, \mathbf{x}) = Q(\mathbf{x})$ and $g(1, \mathbf{x}) = \tau_3 \otimes \mathbb{1}_{2R}$. Noting that $\pi_2(\text{O}(4R)) = 0$, we allow $g(x_0, \mathbf{x})$ to leave the coset space and belong to the orthogonal group, which makes it always possible to find a deformation. In the final step we employ the time reversal constraint to extend the mapping from the half to the full 3-torus (see Section S3 C for details). The resulting mapping is again characterized by a winding number, and it can be verified (see Section S3 C) that integrals over positive and negative half tori, contribute equally to the winding. This allows us to define half of a WZW action,

$$\Gamma[g] = \frac{1}{24\pi} \int_{\mathcal{M}} \text{tr}(\Phi_g \wedge \Phi_g \wedge \Phi_g), \quad (\text{S27})$$

with $\Phi_g \equiv g^{-1} dg$ and integration over half the 3-torus $\mathcal{M} = [0, 1] \times [-1, 1]^2$. The above action is defined up to multiples of 2π , and the right hand side here recalls that the WZW function only depends on the boundary value, i.e. is (modulo 2π) uniquely determined by the original mapping $Q(\mathbf{x})$. Notwithstanding the multi-valuedness of individual terms, the combination of both contributions, Eq. (27), is unambiguously defined $e^{-S_{\text{top}}[Q]} = \pm 1$.

Again we notice that the action Eq. (S27) and coupling constant Eq. (S26) are largely conditioned by the same (symmetry) principles, and refer to Sections S3 A, S3 C, and S3 E for additional details on the construction.

Explicit parametrization:—To demonstrate the topological nature of the protocol Eq. (20) we again concentrate on the mapping induced by $U_{\mathbf{k}}$. We introduce the third momentum s that interpolates from $U(k_0 = 0, \mathbf{k}) = U_{\mathbf{k}}$ and $U(k_0 = \pi, \mathbf{k}) = \sigma_0$, which is clearly trivial, and compute the winding number from T^3 to $SU(2)$ to determine whether the model at $k_0 = 0$ is topologically non-trivial. For that we compute the winding number of $q = (k_0, \mathbf{k}) = \sigma_2 U(k_0, \mathbf{k})$,

$$\theta = \frac{1}{12\pi} \int_0^\pi dk_0 \int d^2\mathbf{k} \epsilon^{\mu\nu\rho} \text{tr}(q^\dagger \partial_\mu q q^\dagger \partial_\nu q q^\dagger \partial_\rho q), \quad (\text{S28})$$

using the following parametrization [45]

$$U(k_0, \mathbf{k}) = \frac{U_{\mathbf{k}} - i \tan(k_0/2) \sigma_3}{\sqrt{1 - 2u_3 \tan(k_0/2) + \tan^2(k_0/2)}}. \quad (\text{S29})$$

As one easily checks, the time-reversal condition, $\sigma_2 U^T(k_0, \mathbf{k}) \sigma_2 = U(-k_0, -\mathbf{k})$, in the extended 3d Brillouin zone is satisfied. With the help of this parametrization we obtain

$$\begin{aligned} \theta &= \int_0^{+\infty} dz \int d^2\mathbf{k} \cos^2(k_1/2) \cos^2(k_2/2) \\ &\times \frac{(3 - \cos k_1 - \cos k_2 + \cos k_1 \cos k_2)}{2\pi (1 + z^2 - z \sin k_1 |\sin k_2|)^2} = \pi, \end{aligned} \quad (\text{S30})$$

where the variable $z = \tan^2(k_0/2)$ was introduced. To evaluate this integral one may check that after $k_1 \rightarrow -k_1$ and $z \rightarrow -z$ the former doesn't change. Thereby extending z -integration over the full real axis (with factor 1/2) one may complete it using residues. The remaining integration over momenta $k_{1,2}$ eventually brings us the angle $\theta = \pi$.

E. Derivation of AII topological term

We next derive the topological action Eqs. (S21) and (S22), starting out from the fermionic action S_2 , given in Eq. (S12),

$$S_2 = \frac{1}{2} (\chi_+^T, \chi_-^T) \mathcal{D}[Z] \begin{pmatrix} \chi_+ \\ \chi_- \end{pmatrix}, \quad (\text{S31})$$

where we focus on the limit $\phi_\pm \rightarrow 0$, for which

$$\mathcal{D}[Z] = \begin{pmatrix} s_1 \otimes i\sigma_2 U^\dagger & \tilde{Z}^T \\ -\tilde{Z} & U s_1 \otimes i\sigma_2 \end{pmatrix}. \quad (\text{S32})$$

Recalling the time reversal constraint, $\sigma_2 U \sigma_2 = U^T$, we notice that the matrix \mathcal{D} is anti-symmetric, $\mathcal{D}^T = -\mathcal{D}$,

and Gaussian integration over fermions therefore generates the Pfaffian $\text{Pf}(\mathcal{D})$. As we show next, the topological action Eqs. (S21) and (S22) accounts for the two possible signs of the Pfaffian, that is

$$e^{-S_{\text{top}}[Q]} = \text{sgn Pf}(\mathcal{D}[Z]). \quad (\text{S33})$$

To this end, we first focus on the minimal coset $\mathcal{M}_R = O(4R)/O(2R) \times O(2R)$ with $R = 1$ and $\theta = \pi$. We show that for particular configurations of Q , respectively Z , with nontrivial windings the sign of the Pfaffian is -1 . For topologically trivial configurations, on the other hand, the sign of the Pfaffian is $+1$. Evoking continuity arguments, it then follows that 'sgn Pf($\mathcal{D}[Z]$)' remains fixed for all Q 's within the same topological sector independent of R . Indeed, the 'sgn'-function is discrete but all configurations Q within the same topological sector can be continuously deformed into each other. Before introducing the specific field configuration, we start out with a brief discussion of the geometric structure of the minimal coset space.

Geometric structure of minimal coset space:—Focusing on the minimal case $R = 1$, the matrix Z is a 2×2 matrix with symmetry constraint $\tilde{Z} = -Z^\dagger = s_1 Z s_1$. We then decompose the matrix into diffuson and Cooperon channels, $Z = Z_d + Z_c$, where

$$Z_d = iw_0 s_0 + w_3 s_3 = \begin{pmatrix} iw_0 + w_3 & \\ & iw_0 - w_3 \end{pmatrix}_{RA}, \quad (\text{S34})$$

$$Z_c = iw_1 s_1 + iw_2 s_2 = \begin{pmatrix} & iw_1 + w_2 \\ iw_1 - w_2 & \end{pmatrix}_{RA}. \quad (\text{S35})$$

Here and in the following matrices s_i operate in particle-hole space, and w_i are real numbers. The related T fields are of the form

$$T_{d,c} = \begin{pmatrix} 1 & Z_{d,c} \\ -Z_{d,c}^\dagger & 1 \end{pmatrix} \equiv 1 + W_{d,c}, \quad (\text{S36})$$

where

$$W_d = iw_0 \tau_1 \otimes s_0 + iw_3 \tau_2 \otimes s_3, \quad (\text{S37})$$

$$W_c = iw_1 \tau_1 \otimes s_1 + iw_2 \tau_1 \otimes s_2. \quad (\text{S38})$$

Using that generators W 's are mutually commuting, $[W_d, W_c] = 0$, we next show that $\mathcal{M}_1 \simeq S_2 \times S_2/\mathbb{Z}_2$. To this end, it is instructive to first recall that in the simpler class A the minimal coset is $SU(2)/U(1) \simeq S_2$. In this case the Q -matrix can be parametrized by a unit vector $\mathbf{n} = (n_1, n_2, n_3)$ or, equivalently, by two spherical angles (θ, ϕ) as

$$\begin{aligned} Q &= \mathbf{n} \cdot \sigma = \begin{pmatrix} n_3 & n_1 - in_2 \\ n_1 + in_2 & -n_3 \end{pmatrix}_{RA} \\ &= \tau_3(n_3 - in_2 \tau_1 + in_1 \tau_2) \\ &\equiv \tau_3 e^{-\frac{i}{2}\phi\tau_3} e^{i\theta\tau_2} e^{\frac{i}{2}\phi\tau_3}. \end{aligned} \quad (\text{S39})$$

Alternatively, one can use a rational parametrization which in the minimal case ($R = 1$) uses a single complex variable $w = w_1 + iw_2$ (the identification is achieved by setting $\tilde{Z} = w$),

$$Q = \frac{1}{1 + |w|^2} \begin{pmatrix} 1 - |w|^2 & 2w^* \\ 2w & -(1 + |w|^2) \end{pmatrix}_{\text{RA}}, \quad (\text{S40})$$

and defines the stereographic projection $\mathbf{n}(w)$ from $\mathbb{C} \rightarrow S_2$,

$$n_1 + in_2 = \frac{2w}{1 + |w|^2}, \quad n_3 = \frac{1 - |w|^2}{1 + |w|^2}. \quad (\text{S41})$$

With this class A example in mind, we can use the same mappings to define diffusion and Cooperon spheres. To this end, we define for the diffuson the matrices

$$\Gamma_1^d = \tau_1 \otimes s_0, \quad \Gamma_2^d = -\tau_2 \otimes s_3, \quad \Gamma_3^d = -\tau_3 \otimes s_3, \quad (\text{S42})$$

satisfying $\Gamma_i^d \Gamma_j^d = i\epsilon_{ijk} \Gamma_k^d$, and $W_d = iw_0 \Gamma_1^d - iw_3 \Gamma_2^d$, where Γ_3^d was introduced to complete the underlying $\text{SU}(2)$ algebra. Defining then the diffuson sphere $Q_d = T_d \tau_3 T_d^{-1}$, it can be verified that

$$Q_d = T_d \tau_3 T_d^{-1} = \tau_3 (n_3^d - in_2^d \Gamma_1^d + in_1^d \Gamma_2^d) = \tau_3 e^{-\frac{i}{2}\phi_d \Gamma_3^d} e^{i\theta_d \Gamma_2^d} e^{\frac{i}{2}\phi_d \Gamma_3^d}, \quad (\text{S43})$$

where the unit vector $\mathbf{n}_d = (n_1^d, n_2^d, n_3^d)$ and angles (θ_d, ϕ_d) follow from the stereographic projection

$$n_1^d + in_2^d = \frac{2w_d}{1 + |w_d|^2}, \quad n_3^d = \frac{1 - |w_d|^2}{1 + |w_d|^2}, \quad (\text{S44})$$

with $w_d = w_3 + iw_0$.

For the Cooperon sphere we introduce a different set of $\text{SU}(2)$ matrices mutually commuting with those of the diffuson,

$$\Gamma_1^c = \tau_1 \otimes s_2, \quad \Gamma_2^c = -\tau_1 \otimes s_1, \quad \Gamma_3^c = -\tau_0 \otimes s_3, \quad (\text{S45})$$

satisfying $\Gamma_i^c \Gamma_j^c = i\epsilon_{ijk} \Gamma_k^c$ and $[\Gamma_i^d, \Gamma_j^c] = 0$, and $W_c = iw_2 \Gamma_1^c - iw_1 \Gamma_2^c$. Introducing then the Cooperon sphere $Q_c = T_c \tau_3 T_c^{-1}$, we notice that

$$Q_c = T_c \tau_3 T_c^{-1} = \sigma_3 (n_3^c - in_2^c \Gamma_1^c + in_1^c \Gamma_2^c) = \tau_3 e^{-\frac{i}{2}\phi_c \Gamma_3^c} e^{i\theta_c \Gamma_2^c} e^{\frac{i}{2}\phi_c \Gamma_3^c}, \quad (\text{S46})$$

and the unit vector $\mathbf{n}_c = (n_1^c, n_2^c, n_3^c)$ and angles (θ_c, ϕ_c) can again be obtained via stereographic projection

$$n_1^c + in_2^c = \frac{2w_c}{1 + |w_c|^2}, \quad n_3^c = \frac{1 - |w_c|^2}{1 + |w_c|^2}, \quad (\text{S47})$$

with $w_c = w_1 + iw_2$.

Finally, we can express the full Q -matrix as

$$Q(\mathbf{n}_d, \mathbf{n}_c) = T_c T_d \tau_3 T_d^{-1} T_c^{-1} = Q_c(\mathbf{n}_c) \tau_3 Q_d(\mathbf{n}_d), \quad (\text{S48})$$

and notice that the odd parity properties $Q_{d,c}(-\mathbf{n}_{d,c}) = -Q_{d,c}(\mathbf{n}_{d,c})$ leave a sign-ambiguity $Q(-\mathbf{n}_d, -\mathbf{n}_c) = Q(\mathbf{n}_d, \mathbf{n}_c)$. We thus arrive at the stated isomorphism $\mathcal{M}_1 \simeq S_2 \times S_2 / \mathbb{Z}_2$.

Evaluation of the Pfaffian:—We next specify $Q = Q_d(\mathbf{n}_d)$ and $Q = Q_c(\mathbf{n}_c)$ to non-trivial mappings from the torus T^2 onto diffuson and Cooperon spheres. That is, we choose configurations with finite windings $\Gamma[Q_{d,c}] = \pi$, and show that in these cases the sign of the Pfaffian (S33) is -1 . More specifically, we consider Pruisken's instantons with windings $W = 1$ and -1 . In stereographic coordinates $w = x_1 + ix_2$, respectively, $w = (x_1 + ix_2)^{-1}$, and we show that the WZW action for the configurations indeed give π . To this end, we extend $Q_{d/c}$ to the group element $g(x_0, \mathbf{x}) \in \text{O}(4)$ defined in three dimensions, such that $g(0, \mathbf{x}) = Q_{d/c}(\mathbf{x})$ and $g(\pi/2, \mathbf{x}) = \tau_3$. Such extension can be achieved in two steps. First we introduce

$$g(x_0, \mathbf{x}) = Q_{d/c}(\mathbf{x}) \cos x_0 + i\tau_3 \Gamma_3^{d/c} \sin x_0, \quad (\text{S49})$$

$$g^{-1}(x_0, \mathbf{x}) = Q_{d/c}(\mathbf{x}) \cos x_0 - i\tau_3 \Gamma_3^{d/c} \sin x_0, \quad (\text{S50})$$

and notice that all matrices $\Gamma_i^{d/c}$ satisfy the symmetry condition

$$\bar{\Gamma}_i^{d/c} = C^T (\Gamma_i^{d/c})^T C = -\Gamma_i^{d/c}, \quad C = \tau_3 \otimes s_1, \quad (\text{S51})$$

implying that $\bar{g} = g^{-1}$, i.e. $g \in \text{O}(4)$ as required. In the above parametrization, the final value $g(\pi/2, \mathbf{x}) = i\tau_3 \Gamma_3^{d/c}$ is still different from τ_3 , and in the second step we introduce an additional rotation $e^{-i\psi \Gamma_3^{d/c}} g(\pi/2, \mathbf{x})$ with $\psi \in [0, \pi/2]$ which brings the latter to τ_3 . Notice, however, that this rotation is inessential for the evaluation of the WZW action. Using that we have a one-to-one mapping from the $2d$ space (or torus T^2) onto the sphere S_2 we can evaluate the WZW action as

$$\begin{aligned} \Gamma[g] &= \frac{1}{8\pi} \int_0^{\pi/2} dx_0 \int d^2\mathbf{x} \text{tr}(g^{-1} \partial_{x_0} g [g^{-1} \partial_{x_1} g, g^{-1} \partial_{x_2} g]) \\ &= \frac{1}{8\pi} \int_0^{\pi/2} dx_0 \int_0^\pi d\theta \int_0^{2\pi} d\phi \text{tr}(g^{-1} \partial_{x_0} g [g^{-1} \partial_\theta g, g^{-1} \partial_\phi g]) \\ &= \frac{1}{\pi} \int_0^{\pi/2} dx_0 \int_0^\pi d\theta \int_0^{2\pi} d\phi (\cos x_0)^2 \sin \theta = \pi, \end{aligned} \quad (\text{S52})$$

which shows that the considered mappings $Q_{d/c}(\mathbf{x})$ belong to a non-trivial homotopy class.

Finally, we show that both mappings give negative signs for the Pfaffian. To evaluate $\text{Pf}(\mathcal{D}[Z])$ on the configuration $Q_d(\mathbf{x})$, defined by a unit vector \mathbf{n}_d with non-trivial winding $W_d = \pm 1$, we start out from the explicit

expression of \mathcal{D} in Eq. (S32)

$$\mathcal{D} = \begin{pmatrix} 0 & i\sigma_2 U^\dagger & iw_0 - w_3 & 0 \\ i\sigma_2 U^\dagger & 0 & 0 & iw_0 + w_3 \\ -iw_0 + w_3 & 0 & 0 & iU\sigma_2 \\ 0 & -iw_0 - w_3 & iU\sigma_2 & 0 \end{pmatrix}. \quad (\text{S53})$$

We then subject \mathcal{D} to an orthogonal transformation defined by the matrix

$$B = \begin{pmatrix} 1 & 0 & 0 & 0 \\ 0 & 0 & 0 & 1 \\ 0 & 0 & 1 & 0 \\ 0 & 1 & 0 & 0 \end{pmatrix}, \quad (\text{S54})$$

which swaps the 2nd and the 4th rows/columns. This brings \mathcal{D} into block off-diagonal form,

$$\tilde{\mathcal{D}} = B\mathcal{D}B^T = \begin{pmatrix} 0 & A \\ -A^T & 0 \end{pmatrix}, \quad (\text{S55})$$

$$A = \begin{pmatrix} iw_0 - w_3 & i\sigma_2 U^\dagger \\ iU\sigma_2 & -iw_0 - w_3 \end{pmatrix}. \quad (\text{S56})$$

At this stage we use that

$$\text{Pf}(\tilde{\mathcal{D}}) = \left(\prod_{\mathbf{k}} \det B \right) \text{Pf}(\mathcal{D}) = (-1)^{m(m-1)/2} \det A, \quad (\text{S57})$$

where m is the size of the matrix A . In the given case $m = 4M$ with M some integer, and the sign reduces to $+1$. Similarly, each generic momentum \mathbf{k} has its TRS image $-\mathbf{k}$, and the number of time-reversal invariant momenta is 4, implying that a negative determinant $\det B = -1$ plays no role. Finally, upon introducing the complex field $w_d(\mathbf{x}) = w_3(\mathbf{x}) + iw_0(\mathbf{x})$, the evaluation of $\det A$ can be reduced to

$$\begin{aligned} \det A &= \det \begin{pmatrix} -w_d^\dagger & i\sigma_2 U^\dagger \\ iU\sigma_2 & -w_d \end{pmatrix} = \det \begin{pmatrix} iU\sigma_2 & -w_d \\ -w_d^\dagger & i\sigma_2 U^\dagger \end{pmatrix} \\ &= \det(1 + U^\dagger w_d U w_d^\dagger). \end{aligned} \quad (\text{S58})$$

This is a familiar form, we already encountered previously in the derivation of a class A action, see Ref. [28]. In particular, the sign of this determinant can be defined

via the (imaginary) Pruisken action,

$$\begin{aligned} \text{sgn}(\det A) &= \exp \left\{ \frac{\theta}{16\pi} \int d^2 \mathbf{x} \epsilon^{ij} \text{tr}(Q_d \partial_i Q_d \partial_j Q_d) \right\} \\ &= e^{i\theta W_d} = e^{i\theta} = -1, \end{aligned} \quad (\text{S59})$$

where the very last relation holds if $U = U_{\mathbf{k}}$ is topologically non-trivial with $\theta = \Gamma[\hat{U}_{\mathbf{k}}] = \pi$. This validates the representation of the topological term as the product of two WZW terms in momentum and real space: when the configuration of field Q_d is nontrivial, the Pruisken term counts its winding in $2d$ space, and as shown in Eq.(S52), the WZW term is identically nontrivial. Provided that the Floquet operator has finite winding, and any nontrivial content of a field configuration $Q = Q_c(\mathbf{n}_c)\tau_3 Q_d(\mathbf{n}_d)$, can be smoothly deformed into the diffuson or Cooperon sector, $Q_d(\mathbf{n}_d)$ respectively $Q_c(\mathbf{n}_c)$, the topological term coincides with the sign-factor ‘sgnPf(D[Z])’, as we set out to show.

We conclude this section by completing the Cooperon part of the derivation.

The evaluation of the Pfaffian for a Q -matrix with non-trivial twist in the Cooperon channel proceeds along the same lines. In this case the antisymmetric matrix \mathcal{D} simplifies to

$$\mathcal{D} = \begin{pmatrix} 0 & i\sigma_2 U^\dagger & 0 & iw_1 - w_2 \\ i\sigma_2 U^\dagger & 0 & iw_1 + w_2 & 0 \\ 0 & -iw_1 - w_2 & 0 & iU\sigma_2 \\ -iw_1 + w_2 & 0 & iU\sigma_2 & 0 \end{pmatrix}, \quad (\text{S60})$$

and the orthogonal transformation that exchanges 2nd with 3rd columns/rows brings it to the block off-diagonal form,

$$\begin{aligned} \tilde{\mathcal{D}} &= \begin{pmatrix} 0 & A \\ -A^T & 0 \end{pmatrix}, \\ A &= \begin{pmatrix} i\sigma_2 U^\dagger & iw_1 - w_2 \\ -iw_1 - w_2 & iU\sigma_2 \end{pmatrix}. \end{aligned} \quad (\text{S61})$$

With a spatially dependent complex field $w_c(\mathbf{x}) = w_1(\mathbf{x}) + iw_2(\mathbf{x})$ the Pfaffian becomes

$$\begin{aligned} \text{Pf}(\tilde{\mathcal{D}}) &= \det A = \det \begin{pmatrix} i\sigma_2 U^\dagger & iw_c \\ -iw_c^\dagger & iU\sigma_2 \end{pmatrix} \\ &= \det(1 + U w_c U^\dagger w_c^\dagger), \end{aligned} \quad (\text{S62})$$

which, similar to the diffuson channel, gives a negative sign for the Pfaffian

$$\begin{aligned} \text{sgn}(\det A) &= \exp \left\{ \frac{\theta}{16\pi} \int d^2 \mathbf{x} \epsilon^{ij} \text{tr}(Q_c \partial_i Q_c \partial_j Q_c) \right\} \\ &= e^{i\theta W_c} = e^{i\theta} = -1, \end{aligned} \quad (\text{S63})$$

provided topological angle $\theta = \pi$, cf. Eq. (S59).